ISSN 1070-3632, Russian Journal of General Chemistry, 2012, Vol. 82, No. 12, pp. 2034–2059. © Pleiades Publishing, Ltd., 2012.
Original Russian Text © J.R. Hernández Carucci, K. Eränen, T.O. Salmi, D.Yu. Murzin, 2011, published in Rossiiskii Khimicheskii Zhurnal, 2011, Vol. 55, No. 2, pp. 16–33.

Gas-Phase Microreactors as a Powerful Tool for Kinetic Investigations

J. R. Hernández Carucci, K. Eränen, T. O. Salmi, and D. Yu. Murzin

Laboratory of Industrial Chemistry and Reaction Engineering, Process Chemistry Center, Åbo Akademi University, Biskopsgatan 8, Turku/Åbo, FI-20500 Finland
e-mail: johernan@abo.fi

Received May 5, 2011

Abstract—The purpose of this review was to show the versatility of gas-phase microreactors for the determination of kinetics of chemical systems. Precise kinetic models were demonstrated for two industrially relevant cases: (a) the continuous selective catalytic NO reduction by hydrocarbons in the excess oxygen at 150–550°C and (b) the catalytic production of ethylene oxide, one of the most important intermediates in the world.

DOI: 10.1134/S1070363212120250

INTRODUCTION

Microreaction technology has been developed during the last decades, representing today an important alternative to conventional macroscopic systems. Microreactors are generally defined as miniaturized reactor systems that exhibit dimensions in the sub-millimetre range, where chemical reactions usually take place in multiple parallel channels with diameters that do not exceed the free path of the molecule for gas-phase reactions [1].

Microreaction systems can be constructed as integrated systems or from single components including basic units such as reactors, mixers, heat exchangers or separators, all in the micrometer scale. Integrated microreaction systems have a more complex design, where multiple components are assembled to form complete units with fluid channel diameters in sub-millimeter scales, finding macroscopic channels only at the end and beginning of the whole system [2].

Regarding microfabrication techniques used for the manufacture of microdevices, they are mostly developed from the field of micro-electromechanical systems. These methods involve the use of lithography, electroplating and molding to design the reactors of materials, such as silicon, quartz, polymers, and metals. Because of the main features of microreactors, they have been recognized in recent years as novel tools in chemistry and chemical process industry, as well as biochemistry and drug development. In addition, the integration of microreactors with miniaturized chemical devices for chemical analysis opens a wide range of applications in combinatorial chemistry, high-throughput screening of catalysts, and operation conditions, as well as in advanced studies of reaction kinetics and mechanisms [3]. Figure 1 shows the different scales of microreactor technology.

Advantages and Challenges of Microreactors

The advantages of microreactors have been previously demonstrated and found to be vast. The main impact of microreactors focuses on intensifying the mass and heat transfer, as well as improving the flow pattern [1]. The key for defining these features is the high surface-to-volume ratios exhibited by microdevices, which tend to be 100 to 500 times higher than conventional laboratory vessels. Many studies have focused on the advantages of using microreactors [3–11] over more traditional approaches, and a summary of these benefits are presented below.

Firstly, the improvement of the flow patterns can be understood by means of the dependency of fluid flow characteristics on the scale. For microfluidic systems, the flow behavior is essentially laminar having a direct consequence on the backmixing. It is known that mixing of molecules is achieved by diffusion and that the time scale of diffusive mixing increases with the

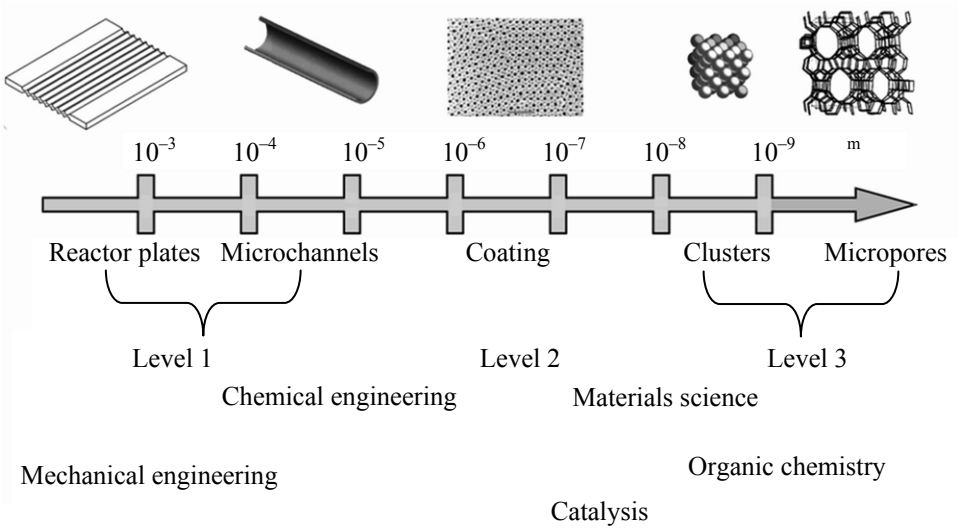

Fig. 1. Different scales in microreactor technology (obtained from E. Rebrov, Queens University, Belfast).

characteristic dimensions of the reactor. For instance, in microreactors, the diffusion distances drop below 100 μm and, as a result, the mixing times become very small, allowing rapid formation of a homogeneous reactant mixture at the initiation of the reaction [4].

On the other hand, the high heat transfer, which is also a consequence of reduced thermal masses, allows exothermic or high temperature reactions to be carried out in an efficient and controllable manner. Moreover, as a catalyzed reaction is performed, the efficient heat transfer enables a good utilization of the catalyst during highly endothermic and exothermic reactions and the formation of hot spots is avoided [5]. Because higher reaction temperatures are achieved, the reaction volume and the amount of catalyst can be reduced significantly. In addition, since the small diameters of the reactor channels guarantee a short radial diffusion time, a narrow residence time distribution is obtained leading to a high selectivity of the desired intermediate during consecutive processes. The use of microstructured reactors also leads to a principally straightforward scale-up, given that there is no need to transfer the reaction from the laboratory to a pilot plant [6]. The strategy is based on the principle of numbering up, and thus in the connection between an increased number of microdevices and the internalization of a high number of channels [7]. Mixing and flow pattern in the reactor is crucial in performing chemical processes, for which high selectivities of the desired products are required. In microstructured systems, the flow pattern can in principle be tailored for each reaction system, so that the product distribution is optimized.

For heterogeneously catalyzed reaction systems, the diffusion resistance in the porous catalyst layer is a bottleneck, since it retards the reaction rate in most cases. Very thin catalyst layers (less than 100 μm) are used in microreactors, which minimizes the diffusion resistance and improves the overall effectiveness of the catalyst. In addition, screening of new catalyst materials is essentially enhanced by the use of microreactors, since the standard pressing-crushing-sieving procedure in testing of catalyst particles is avoided in the use of microreactors: the walls of microreactors can be coated with thin catalyst layers (less than 50 μm in thickness). This suppression of diffusion resistance leads to a considerable minimization of the process equipment, i.e. to process intensification. Several micro- and millireactors devices have been developed at Åbo Akademi University during recent years.

It is also expected that in the future, dangerous and unstable chemicals are not going to be transported on the roads, but manufactured on site, where they are needed. With microreactors, fine chemicals can be produced in a continuous mode, thus enabling stable operation conditions and a high product quality. It is expected that many chemical processes carried out batchwise today will be performed in continuous microreactors in the future.

Modern process design is based on mathematical modelling, simulation and optimization. Even though large steps forward have been taken in this area the effort required is still huge, particularly in scaling-up of new processes. Advanced calculation methods are applied in various steps in the process development

from laboratory to bench, pilot and plant scales. Sometimes it is possible to make a big leap from laboratory to plant scale, but more typically separate experimental activities along with mathematical modelling are required for the different scales. A lot of time and money is consumed. Microstructured devices are claimed to be of great help here: as the development work has once been done for a microstructured equipment, the expansion to the plant scale can be done by coupling several microdevices in parallel, and in this way, reach the required production capacity. The traditional concept of scale-up is replaced by number-up. Finally, microreactors are valuable in increasing the chemical process safety. Indeed, continuous operation and small reagent volumes are used and explosive reactions are conducted in a confined environment. These devices offer a better control to prevent temperature runaway.

In summary, compared with the macroscale, microreactors engender significant advantages in terms of speed, throughput, yield, selectivity, and control. All are directly facilitated by reactor downscaling and associated improvements in the mass and heat transfer [6].

Nevertheless, there are still challenges for microreaction technology, e.g., problems with liquid-liquid mixing, associated costs and fouling phenomena that might occur when handling solids inside the microchannels [6]. Additionally, the concept of scale-up by replication of many units, which appears simple, could still present new challenges, e.g., challenges in fluid handling, complex reactor monitoring and control as the parallel array size grows to a large number of reactors [3]. Furthermore, for the case of heterogeneous catalysis, deposition of the active phase is challenging (uneven coatings, non-uniform metal distribution on the support, low adherence, and catalyst deactivation) and needs to be optimized. Consequently, in order to move from laboratory scale to chemical production, still some development is needed and multiple research efforts are required [3]. Moreover, the use of microreactors for multiphase systems has turned out to be extremely difficult and even the efforts to obtain reproducible experimental results is a challenge as such. The problem of multiphase operation in microreactors is related to the mixing of two phases in microscale and to the ability to control the hold-ups of the phases and the bubble sizes of the discontinuous phase. The distribution of the flow into the parallel channels of a microreactor remains in most cases unknown, which leads to a paradox: calculations based on the theories of chemical reaction engineering (CRE) show for a particular reaction system, which one is the optimal flow pattern (often it is close to plug flow), but the microreactor device creates a residence time distribution (RTD), which is less favorable than the theoretically calculated optimal one. Practical experience has also shown that it is in many cases exaggerated to go down to microscale in diminishing the size, but the use of milliscale equipment is sufficient enough. In milliscale equipment, the flow pattern is more easily predicted, since the macroscopic laws of fluid mechanics can be directly applied.

Last but not least: The currently available microreactor and separator systems are still expensive. This problem is surmounted as microdevices are used in laboratory scale for research purposes (catalyst screening, determination of reaction kinetics and equilibria), for which a limited number of microdevices are needed and they are financed with public funding. Industrial production, on the other hand, must be economic and profitable. The number-up principle in its simplest form implies that a lot of microreactors are placed in parallel. A system built in this way contains a lot of steel per volume, much more than a conventional unit, becomes expensive. Thus it is of great interest to try to find less expensive and more flexible manufacturing technologies for micro-structured devices.

Manufacturing technology alone is, nonetheless, not enough for the success of microprocess technology, but it should be combined with a deep knowledge of process technology, which includes the elements of materials science, chemical kinetics and thermodynamics, mass and heat transfer phenomena as well as flow modelling.

Gas-Phase Microreactors

In this section, we give an example of a gas-phase microreactor specially designed for research purposes. Such gas-phase microreactor was designed at Åbo Akademi and the parts were purchased from the Institut für Mikrotechnik Mainz (IMM). The device consists of a two-piece cubic chamber with two inlets and one outlet, each with a tube diameter of 710 μm. The lower part of the chamber has two recesses, each filled with a stack of ten microstructured platelets, which are connected by a diffusion tunnel. The first stack contains a total of ten mixing platelets with nine semicircular channels of different radii but with a common centre. They are arranged in the stack in such

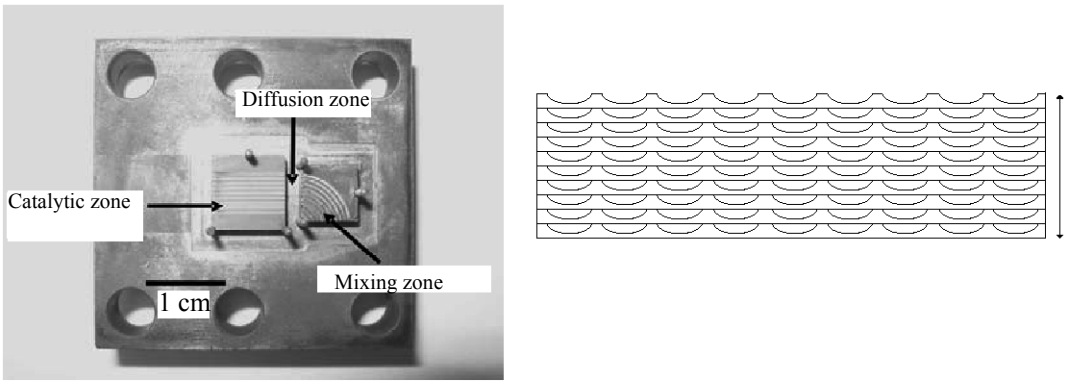

Fig. 2. (Left) Microreactor chamber (mixing and catalytic zones) and (right) scheme of the reactor configuration (10 stacked microplates, catalytic zone).

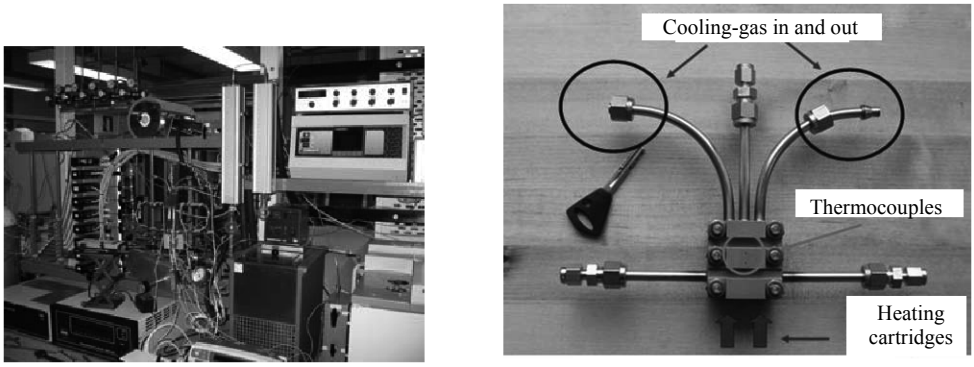

Fig. 3. (Left) Experimental set-up of the microreactor and (right) detailed view of the microreactor.

way that they meet the two inlets in alternation. The second stack consists of ten rectangular platelets with nine parallel shallow microchannels (Fig. 2, left, diameter 460 μm, length 9.5 mm, depth 75 μm) of a pure metal or coated with a suitable catalyst. Figure 2, right, shows a scheme of the plates' configuration inside the microreactor. A maximum gas flow of 80 ml min^{-1} is permitted. Pressures and temperatures up to 50 bar and 600ºC, respectively, can be achieved. Figure 3 shows a basic experimental set-up for most of the experiments (left) and a top view of the microreactor chamber (right). The idea of this study is to demonstrate the versatility of microreactors for advanced kinetic studies. Two industrially-relevant reaction examples will be taken into consideration: (a) catalytic abatement of exhaust gases and (b) catalytic production of ethylene oxide.

Active-Phase Introduction

The technology of supported catalysts is well-known in general, but deposition of small microreactor channels with the support material and the catalytically active metal is still challenging. The microreactor walls were successfully washcoated with various supports and active metals, such as silver and gold, as well as Cu on zeolites [12]. Silver supported on alumina catalysts were used in the catalytic abatement of the exhaust from biofuels combustion. Cu/ZSM-5 has also been synthesized and was tested for the hydrocarbon assisted selective catalytic reduction of NO_x with good activities and NO_x-to-N_2 selectivities (Fig. 4, [12]). For the production of one of the largest intermediates in the chemical industry, ethylene oxide, pure silver microplates were tested, obtaining selectivities up to 55% (Fig. 5, [13]). On the other hand, gold catalysts have also been washcoated, but their full potential has not yet been exploited. Such catalysts are suited, for instance, for isomerisation and oxidation reactions.

Several silver/alumina catalysts were prepared, mainly by washcoating and impregnation. Stainless-steel microplates (Fig. 2, catalytic zone) were washcoated with alumina support (A-201, La Roche)

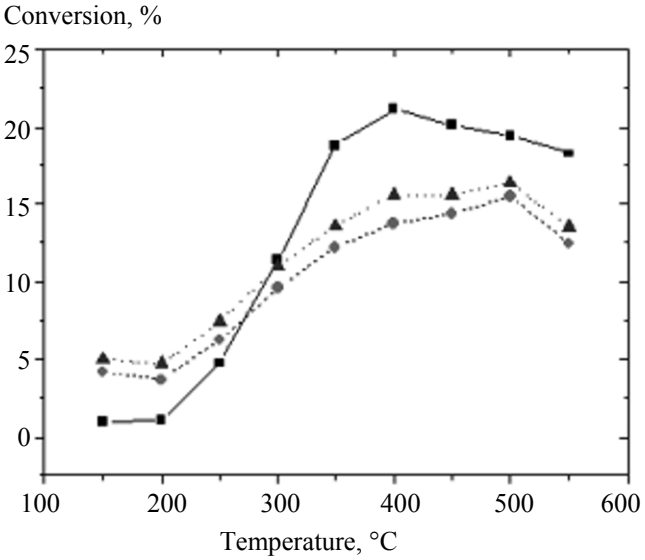

Fig. 4. NO-to-N_2 conversion on the SCR of NO_x with hexadecane, with different catalyst configurations: (■) 1.9 wt % Ag/Al_2O_3, (●) 3 wt % Cu-ZSM-5, and (▲) 1.9 wt % Ag/Al_2O_3+ 3 wt % Cu-ZSM-5. Reaction conditions: 500 ppm NO, 188 ppm $C_{16}H_{34}$, 6 vol % O_2, 12 vol % H_2O (for 1.9 wt % Ag/Al_2O_3 only).

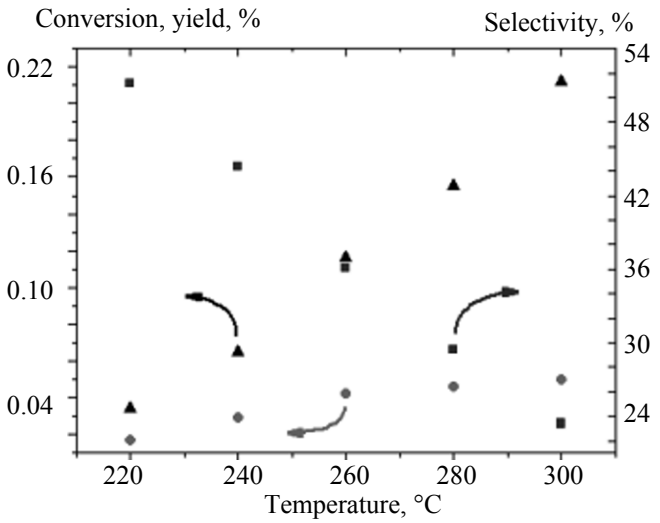

Fig. 5. Effect of temperature on (■) conversion, (●) yield, and (▲) selectivity on the production of ethylene oxide over pure silver microplates. Reaction conditions: 20 vol % ethylene, 10 vol % oxygen, total flow 6 ml min^{-1}.

and further impregnated with silver by using a conventional stirrer. An example of the catalyst preparation techniques for microreactor elements is provided in Fig. 6: the microreactor elements contain the support material (e.g. alumina or silica), after which the active metal component is fixed on the support by wet impregnation: the microreactor plates are fixed on a rotating impeller, which is immersed in the impregnation liquid. By changing the impregnation time and the metal ion concentration in the liquid, catalysts with different metal contents and metal particle sizes can be prepared (Fig. 6). Before the deposition of the washcoat, the catalyst plates of the microreactor were cleaned from impurities by using the method described by Howell and Hatalis [14]. First, the plates were immersed in acetone for a few minutes and rinsed with deionised water. They were further immersed in a solution of 5:1:1 distilled water, hydrogen peroxide (29–32%, Merck), and ammonium hydroxide (32%, Sigma-Aldrich) for 5 min and rinsed with distilled water. Finally, the plates were immersed in a solution of 5:1:1:1 distilled water, hydrogen peroxide (29–32%, Merck), phosphoric acid (85%, FF-Chemicals), and acetic acid (99% glacial, J.T. Baker) in an ultrasonic bath for 5 min, rinsed with distilled water and then dried. All the plates were calcined for two hours at 800°C before the coating process.

The washcoating method consisted on covering the channels with a suspension powder, a binder, acid and water as the main components. In particular, 20 g of ground gamma-alumina (A-201, La Roche) were suspended in 75 g of deionised water, 5 g polyvinyl alcohol MOWIOL 40-88 (Aldrich, MW 205,000) and 1 g of acetic acid. The suspension was placed on the microplates wiping any excess with a blade. The plates were dried during two hours at 100°C and further calcined at 550°C in air for 3 h.

The alumina-coated plates were further impregnated by silver in silver nitrate solutions (J.T. Baker) at studying the effect of the silver nitrate concentration and impregnation time on the metal loading. 0.011, 0.022, and 0.04 M solutions were used and the plates were left to impregnate at 12, 24, and 48 h at room temperature and mild stirring. After impregnation, the plates were again dried during three hours at 100°C and further calcined for three h at 550°C in air. The effect of the impregnation time and precursor concentration on catalytic activity was studied extensively [12].

Other materials have also been washcoated on the microchannels. Zeolite-based catalysts have attracted the interest of scientist in the last decades. Zeolites, due to their unique properties of shape selectivity, uniform channel system, thermal stability, ion-

exchange capacity, coke resistance and acidity, have found application as catalysts in several processes, from petroleum industry to fine chemicals. It is certainly possible to coat different zeolite structures such as Beta, ZSM-5, Mordenite, and Y directly into the microchannels. The silica-to-alumina ratios of these structures can be adjusted during the synthesis for obtaining zeolite-based microreactor elements with varying acidities. For example, Cu-ZSM-5 can be coated on the microchannels. The procedure is briefly described as follows: a mixture containing a commercial zeolite powder Na-ZSM-5 (Degussa, Si/Al 22.6) and alumina A-201, La Roche (ratio 1:3) was ground together and placed under water, with a 0.9 wt % solution of nitric acid at 50°C. After homogenization, the plates were introduced in the solution and were left to impregnate for 4 h with mild stirring. The plates were further dried at 100°C for 1 h and calcined in air at 550°C for 3 h. The metal (Cu) was introduced by ion-exchange using a 0.05 M copper acetate solution during 24 h with mild stirring. The plates were again dried at 100°C for 2 h and further calcined at 550°C for 2 h. Another procedure used for the Cu-ZSM-5 coating was the one presented in [15] plus metal modification. Zeolite (Degussa, Si/Al 40), 20 g, was placed in a 0.05 M copper acetate solution during 24 h at room temperature with mild stirring. The resulting catalyst was filtered, washed with distilled water, dried at 110°C, and calcined at 400°C. A suspension with 20 g of the prepared catalyst, 75 g of deionised water, 5 g of polyvinyl alcohol, and 1 g of acetic acid was prepared. The binder was dissolved in water under mild stirring at 60°C for 2 h, and the resultant solution was kept overnight at the same temperature. The catalyst powder and acetic acid were added successively, without stirring. The resulting mixture was stirred for 2 h at 60°C and left successively for five days without heating. The suspension was then drawn

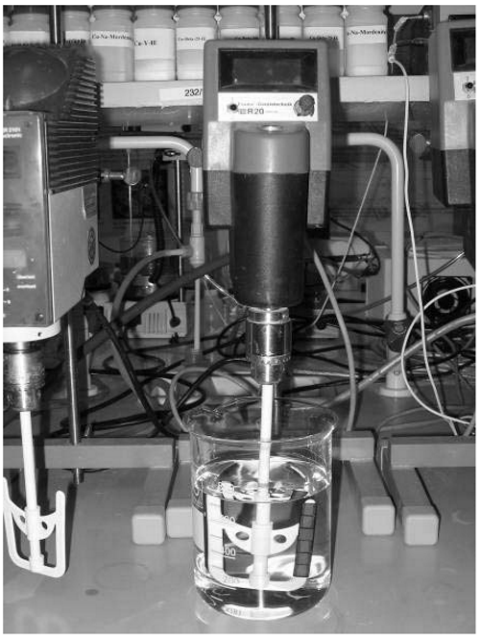

Fig. 6. Impregnation of the microplates using a conventional stirrer.

with a syringe and used to fill the microchannels (Fig. 7, right), dried for 3 h at 100°C, and further calcined for 3 h at 550°C in air [15]. Figure 7, left) shows the stirring and deposition steps of the catalyst on the microplates (right) of this procedure. The coated plates were tested for the selective catalytic reduction of NO_x with hexadecane (Fig. 4).

Characterization of Microplates

Characterization techniques tend to be different for washcoated elements. Still, many researchers rely on classic Scanning Electron Micrograph (SEM) images, although newer and more advanced techniques, e.g., X-ray Photoelectron Spectroscopy (XPS) and Laser Ablation Inductively Coupled Plasma Mass Spectrometry (LA-ICP-MS) are also used. These two

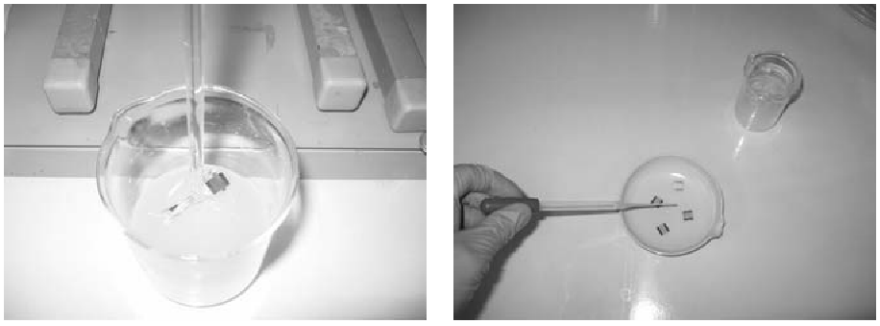

Fig. 7. Preparation of the Cu-ZSM-5-coated plates.

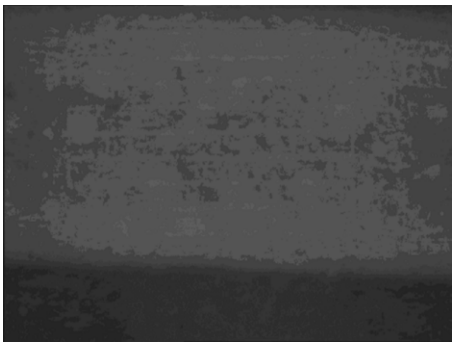

Fig. 8. LA-IPC-MS: laser track on a microplate.

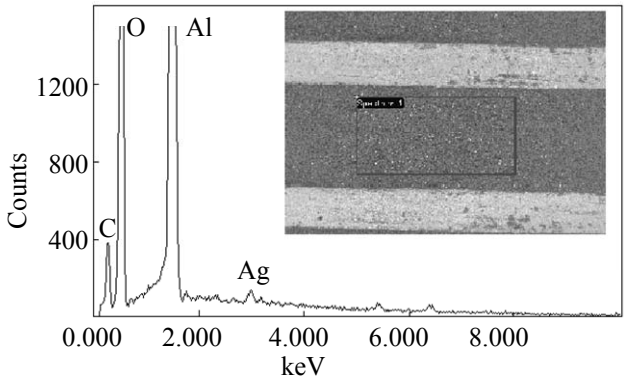

Fig. 9. Quantitative analysis of an Ag/alumina coated microplate fragment with SEM-EDXA. Accelerating voltage: 15 keV; take off angle: 34.9795°; live time: 90s; dead time: 25.321.

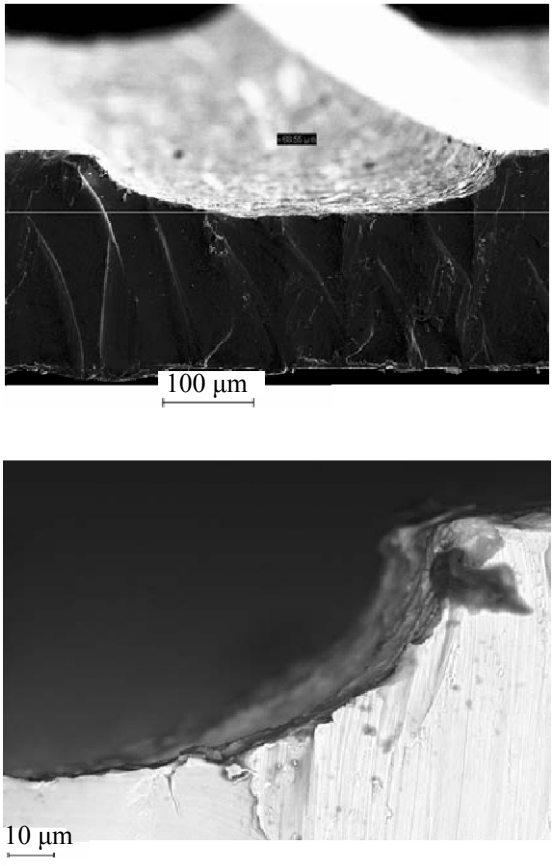

Fig. 10. SEM images of (top) an uncoated channel (200×) and (bottom) an Ag/alumina coated channel (1000×).

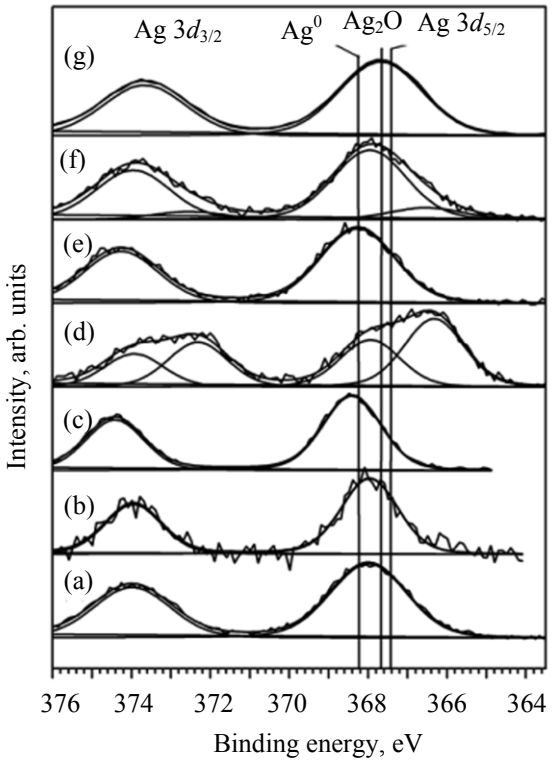

Fig. 11. Ag $3d_{5/2}$ lines from different samples (see notes to Table 2 for nomenclature).

methods, together with XPS, are briefly presented below. The characterization of the Ag/alumina catalyst through LA-ICP-MS was carried out by a Merchantek UP-213 (New Wave Research, USA) LA system coupled to a PerkinElmer SCIEX ICP-MS instrument (Elam 6100 DRC Plus). The sample surface was irradiated with deep-UV (213 nm) output from a frequency-quintupled Nd: YAG (neodymium-doped yttrium aluminium garnet crystal) laser. The laser light couples to the surface of the sample, causing very rapid heating, which, in turn, causes the matrix to be volatilized or ablated. This ablated material is then carried to the ICP-MS in an argon carrier gas stream for analysis. The scan speed used during the analysis was 20 μm/s, the laser energy output was 50%, and the spot size was 8 μm. Figure 8 shows a typical trajectory

Table 1. Binding energies and estimated oxidation states of the metals

Catalyst[a]	Al 2*p* (eV)	C 1*s* (eV)	O 1*s* (eV)	Ag 3$d_{5/}$ (eV)	State	Au 4$f_{7/2}$	State
A	74.6	285.0	531.1	368.0	Ag^0	–	–
B	74.6	284.8	532.3	368.2	Ag^0	–	–
C	74.0	284.6[b]	531.1	368.1	Ag^0	–	–
D	74.6	284.7	530.6	366.4 (58%) 368.0 (42%)	Ag^+ Ag^0	–	–
E	74.6	284.7	531.7	368.6	Ag^0	–	–
F	74.6	284.8	530.7	–	–	84.2	Au^0
F ion etch	74.6	–	530.6	–	–	–	–
G	74.6	284.5	530.6	366.5 (14%) 368.0 (86%)	Ag^+ Ag^0	–	–
H	73.8	284.6[b]	531.1	368.1	Ag^0	–	–
H ion etch	74.6	284.1	530.3	366.9 (63%) 368.0 (37%)	Ag^+ Ag^0	–	–
I	74.6	285.2	531.3	368.3	Ag^0	–	–

[a] Nomenclature for the XPS analysis: (A) Ag/alumina (0.04 M, 24h); (B) Ag/alumina (0.04 M, 12h); (C) Ag/(alumina + ionic liquid); (D) Ag/alumina (0.022 M, 24h); (E) Ag/alumina (0.022 M, 12h); (F) Au/alumina (deposition); (G) Ag/alumina (0.04 M, 48h); (H) Ag/alumina (0.011 M, 48h); (I) Ag/alumina (0.022 M, 48h). [b] Low signal-to-noise ratio.

of the laser beam in the microplate. One of the disadvantages of the method is that it is highly invasive, destroying the catalyst coating since the laser beam evaporates the components of the washcoat.

The metal content was also investigated by SEM-EDXA, giving results similar to those obtained by LA-ICP-MS. The SEM images were taken on the scanning electron microscope system Leo 1530 Gemini manufactured by Zeiss. The Leo 1530 presents an acceleration voltage of U_{acc} 0.2–30 kV and a field emission gun (FEG) resolution of 1.0 nm at 20 kV, 2.5 nm at 1 kV, and 5 nm at 0.2 kV. The analyses were carried out by an energy dispersive X-ray detector (EDX, Thermo Noran VANTAG-ESI, 120 kV). Figure 9 presents an example of the quantitative analysis of the specific surface area of a microchannel. The silver content was determined to be ca 1.4 wt % with respect to Al_2O_3. Furthermore, Fig. 10 shows the SEM images of (top) an uncoated and (bottom) a coated channels. The thickness of the catalytic layer was found to be between 10 and 20 μm (Fig. 10, bottom).

Finally, XPS was also used for understanding the catalytic coatings. A Perkin-Elmer 5400 ESCA spectrometer was used with monochromatized AlK_α radiation (photon energy 1486.6 eV) and a pass energy value of 35 eV. Samples were in contact with ambient air prior to the analysis and the examination was made from the surface of the microplate without any additional chemical or physical treatments. A low-energy electron gun (flood gun) was used to stabilize the charging that arises from loss of photoelectrons during X-ray bombardment. To calibrate the binding energy axis accurately, carbon 1*s* line at 284.6 eV was used [16]. Examples of the XPS analysis for different catalysts are shown in Table 1. In the line-fitting procedure, intensity ratios of $2p_{3/2}$:$2p_{1/2}$, $3d_{5/2}$:$3d_{3/2}$ and $4f_{7/2}$:$4f_{5/2}$ lines were kept fixed at their theoretical values (2:1; 3:2; 4:3) and a mixture of Gaussian and Lorentzian line shapes was used. In silver catalysts with high loadings, Doniach-Šunjić line shape was used to fit slightly asymmetric Ag 3*d* lines. Sensitivity factors used in determining atomic concentration ratios for Ag 3*d*, Al 2*p*, Au 4*f*, C 1*s*, Cu 2*p* and Si 2*p* were 5.198, 0.193, 5.240, 0.296, 4.798, and 0.283, respectively [16].

Silver was found to be in a slightly oxidized state in most cases. Figure 11 shows an example of the Ag $3d_{5/2}$ lines for different Ag and Au catalysts. The

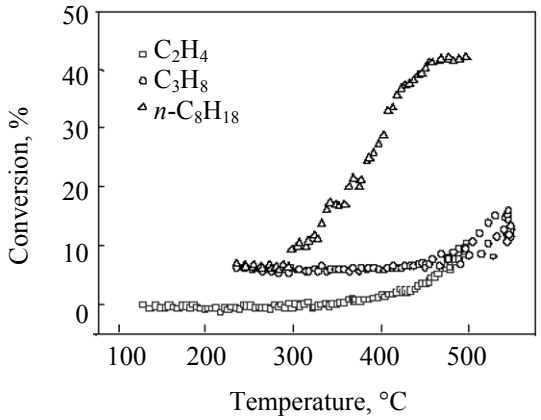

Fig. 12. HC-SCR of NO_x over 1.6 wt % Ag/Al_2O_3-coated microchannels with different hydrocarbons. Reaction conditions: 6 vol % O_2, 0.5 vol % NO, 1.25 vol % C_2H_4/0.83 vol % C_3H_8/0.3125 vol % n-C_8H_{18}.

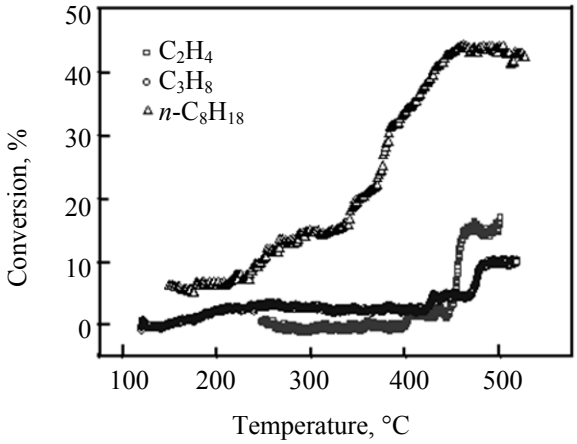

Fig. 13. HC-SCR of NO_x over a 1.9 wt % Ag/Al_2O_3 powder in a minireactor with different hydrocarbons. Reaction conditions: 6 vol % O_2, 0.5 vol % NO, 1.25 vol % C_2H_4/0.83 vol % C_3H_8 /0.3125 vol % n-C_8H_{18}.

results obtained by XPS were in line with previous characterization. The coating of the plates is a challenging and systematic procedure that needs to be optimized. Comparing the preparation of a regular powder catalyst with the impregnation procedure described here, both procedures seem to be equally challenging. It is particularly difficult to obtain a uniform coating with the same catalytic thickness along the microchannels.

Other classical characterization techniques, i.e., nitrogen physisorption, transmission electron microscopy (TEM), gas chromatography combined with mass spectrometry (GC-MS) can also be used for characterizing the microplates. Nonetheless, the analyses need to be performed before the washcoating procedure.

Activity Testing of Microplates

As we mentioned above, two case studies have been considered in this work: (a) the selective catalytic reduction of NO_x (SCR) using hydrocarbons and (b) the ethylene oxide formation.

For the former case, four different hydrocarbons were used: ethylene, propane, *iso*-octane and *n*-octane. As expected, the NO reduction was shown to be sensitive to the temperature and to the number of carbon atoms present in the hydrocarbon. The results obtained in the microreactor were compared to those obtained in a minireactor under similar conditions, i.e., keeping the flow rate/mass of catalyst ratio the same for both cases.

The activity test results over the alumina supported silver catalysts in the microreactor and minireactor in the excess of oxygen are shown in Figs. 12 and 13, respectively, for different hydrocarbons. The HC/NO ratio was kept constant at 5. As previously found [17], this ratio should be between 4 and 6 in order to achieve the maximum conversion in HC-SCR. The results revealed that the reduction capacity of the hydrocarbon at a single temperature, depended on the amount of carbon atoms present in the molecule, i.e., at 450°C, octane exhibited the highest NO_x reduction (almost the same for the case of isooctane, not shown in the figures), followed by propane and ethylene, which showed the lowest activity for both reactor systems [18].

In general, the behaviors of the microreactor and minireactor were similar. However, for the case of the NO reduction with propane, the microreactor exhibited a better reduction compared to that achieved in the minireactor system (Figs. 12 and 13). It is not surprising to have differences in the results between the mini- and the microreactor. Even if the reaction conditions were kept the same, there are still some differences between the systems, e.g., metal loadings, different specific surface area of the washcoats and powders. Moreover, due to the small dimensions in the microchannels, the homogeneous gas-phase reactions are significantly suppressed, with the surface reaction on the catalytic wall being predominant. The gas-phase reactions have been shown to be of importance on the HC-SCR system over Ag/Al_2O_3 [19, 20].

For the case of ethylene oxide production, pure silver microplates were used. Ethylene oxide (EO) is one of the most important organic intermediates with

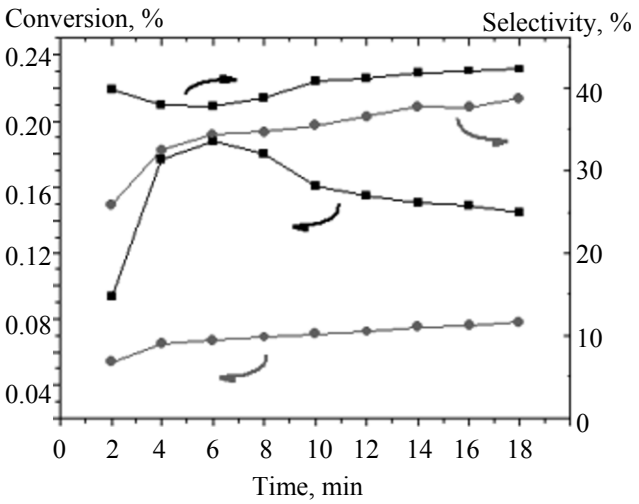

Fig. 14. Effect of pretreatment with oxygen and ethylene on conversion and selectivity on pure silver microchannels. (●) Oxygen pretreatment: 20 vol % O_2 for 20 min at 260°C; total flow 5.4 cm^3 min^{-1}. (■) Ethylene pretreatment: 20 vol % C_2H_4 for 20 min at 260 °C; total flow 5.4 cm^3 min^{-1}. Reaction conditions: 20 vol % ethylene, 10 vol % oxygen, total flow 6 cm^3 min^{-1} at 260°C.

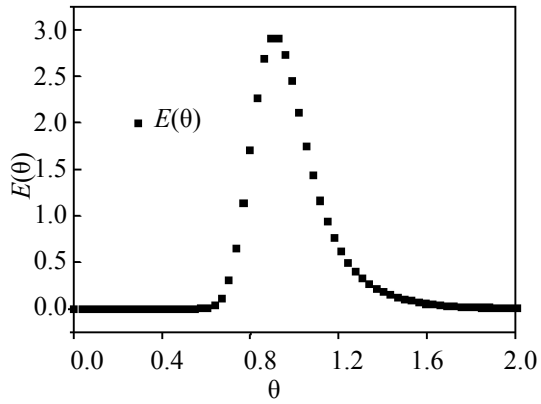

Fig. 15. $E(\theta)$ function for an injected pulse of 0.05 ml argon in nitrogen as carrier gas in an inert microreactor. Volumetric flow rate 8 ml min^{-1}.

an annual global production of roughly 19 million metric tons and it is expected to grow 4.5% per year from 2007 to 2012 [21]. Ethylene oxide is produced industrially based on the direct oxidation of ethylene by using either air or pure oxygen. Silver is the state-of-the-art catalyst with different promoters, for enhancing activity and selectivity towards the desired product (ethylene oxide). Commercially available γ-Al_2O_3-supported catalysts have been reported to achieve conversions from 7 to 65% and selectivities of up to 80% [22]. Current industrial catalysts consist of silver particles deposited on ultrapure (over 99%) aluminium oxide support with a well-defined pore structure (pore diameter 0.5–50 μm) and low specific surface area (< 2 m^2 g^{-1}).

Ethylene oxide can, in principle, be produced on site with the aid of suitable, selective heterogeneous catalysts. This requires, however, a very advanced reactor technology, in which the classical problems of scale-up and operability are circumvented. Such a technology is provided by microstructured devices, particularly gas-phase microreactors, which are inherently safe and have very good operability properties [23, 24].

Nault et al. [25] tried to pretreat the catalyst with oxygen, ethylene, hydrogen and ethylene oxide in order to improve the stability and activity of the catalyst. A similar approach of different pretreatments with oxygen and ethylene was tested in this study, in order to find good stability and activity windows for the catalyst. When pretreating with ethylene, a 20 vol % flow was kept for 20 min at 260°C with a total flow of 5.4 cm^3 min^{-1}. When oxygen was used as a pretreatment gas, the parameters were kept identical. Before starting the experiment, the microreactor was purged with helium for 20 min in both cases.

A peak of ethylene oxide formation was observed after 6 min after beginning the reaction, together with a slight decrease in the selectivity (Fig. 14 [13]), in the case when the silver plates were treated with ethylene. With oxygen as a pretreatment gas, the conversion was gradually increasing from 0.05 to 0.08% after 18 min reaction, while the selectivity toward ethylene oxide changed from 25.9 to 38.7%.

An important difference between the pretreatments was that the conversion for ethylene-treated catalyst was almost double that for oxygen-treated microplates. Similar trends of the catalytic behavior were observed by Nault et al. [25]. They treated first the catalyst overnight with pure oxygen at 200°C and followed it with ethylene treatment. They noted that after an initial activity peak, the catalyst slowly decreased its activity, stabilizing only after 2 h. Additionally, the treatment consecutive of the catalyst with hydrogen and ethylene resulted in further activity enhancement [25]. They presented the possibility that the catalytic sites are, at least, partially reduced, and the pretreatment with ethylene oxide increased the activity of the existing catalytic sites or produced entirely new ones.

Van Santen and Kuipers [26] explain the uniqueness of silver as an ethylene epoxidation

catalyst by two factors: firstly, the bond strength and chemical nature of the adsorbed oxygen, and, secondly, the inability to activate the C-H bond. The latter factor is supposed to limit the catalysts to elements or components not containing transition metals, because these transition metals activate the C-H bonds. Oxygen has to dissociate, but the resulting metal-oxygen bond strength should not be high that epoxidation could be excluded because of thermodynamic reasons. Silver is unique, since oxygen can dissociatively adsorb on its surface and at high oxygen coverage it contains weakly bound oxygen. The relatively weak bond strength of oxygen to silver, thermodynamically allows formation of ethylene oxide upon reaction with ethylene [26].

According to van Santen and Kuipers [26], clean silver surfaces have an initial selectivity to ethylene oxide of approximately 40%, which is relatively low. It can be, however, explained by the low surface oxygen concentration, which enhances the fraction of strongly adsorbed oxygen. The studies by Campbell [27] showed a clean Ag(111) surface had a selectivity of 36–48%, while clean Ag(110) surface has a selectivity of 36–39% towards ethylene oxide formation depending on the reaction temperature.

Kestenbaum et al. [28], while synthesizing ethylene oxide in a catalytic microreactor, used polycrystalline catalytic plates similar to the plates used in this study. Additionally, no promoters were used for enhancing the catalytic reaction. They found that the selectivities of ethylene oxide on polycrystalline silver were about 50%, which does not differ too much from the values reported in the literature for conventional reactors. It was also found that in the microreactor, the selectivity toward ethylene oxide increased as more oxygen was fed to the reactor.

Lee et al. [29] studied the effects of various support materials on silver catalysts. The conclusion was that catalysts with several carriers including γ-Al_2O_3 exhibited a significant activity in ethylene oxide isomerisation and oxidation, and thus they gave only a very poor selectivity toward the ethylene oxide formation or formed only carbon dioxide and water. This was attributed to the surface acidity of the catalysts.

Modeling of Microdevices

In order to design and use microdevices accurately for research and industrial production, the behavior of the gas flow of the reactants and products inside the microchannels has to be characterized and explained. When comparing the flows inside the microchannels with those present in regular-sized reactors, the differences are as follows: (i) The flow in microchannels is usually laminar and turbulent in macrochannels; (ii) The diffusion paths in the microchannels for heat and mass transfer are very small; (iii) A high surface-to-volume ratio prevails in the microchannels, which implies that a high surface ratio effects dominate over volume effects; and (iv) Solid wall materials are important in microchannels, hence, heat transfer by conduction is important.

Non-Reactive Flow Modeling

In chemical reaction engineering, a model capable of simulating the behavior of the process is essential for predicting reactor performance. Moreover, it plays an important role in the process optimization. Because real reactors seldom follow the flow patterns of ideal reactors (the plug-flow and complete backmixing models), a large number of models approximate these ideals with negligible errors [30]. A very informative characterization of the flow pattern is the residence time distribution (RTD). It gives information on how long the various volume elements have been in the reactor. It also provides a quantitative measure on the degree of backmixing within a vessel and thus allows an accurate kinetic modeling of the system as well as the achievement of a desired flow pattern [31].

*Age distribution***.** The elements of fluid take different paths through the reactor; they may require, as well, different lengths of time to pass through the vessel. The distribution of these times is called the exit age distribution (E), or RTD [30]. The RTD is represented by the following equation, in such a way that the area under the curve becomes the unity:

$$\int_0^\infty E dt = 1. \quad (1)$$

In order to evaluate the E-function, it is necessary to resort in an experimental method classed as stimulus-response technique. This technique implies disturbing the system with an inert tracer and then evaluating the response to the stimulus, such as the Dirac δ-pulse, which does not disturb the flow pattern in the vessel, i.e., an inert gas in our case. It is important to recall that a closed vessel is defined as one in which the fluid enters and leaves by plug flow having a flat velocity profile [30].

The relationship between the age distribution function $E(t)$ and the concentration $c(t)$ is given by

$$E(t) = \frac{c(t)}{\int_0^\infty c(t)dt} . \quad (2)$$

Since the distribution is usually characterized by few numerical characteristics, it is important to measure the location of the distribution. Thus, this location is defined as the mean value of the distribution ($\bar{t}$) and is defined by the following equation, which can be expressed as a function of $E(t)$ or for a curve of concentration (c) as function of time (t) [30] in integral and discrete forms,

$$\bar{t} = \int_0^\infty E(t)tdt = \frac{\int_0^\infty tcdt}{\int_0^\infty cdt} \approx \frac{\sum_i t_i c_i \Delta t_i}{\sum_i c_i \Delta t_i}. \quad (3)$$

Additionally, an important descriptive quantity is the width of the distribution, which is characterized by the variance (σ^2), defined as

$$\sigma^2 = \int_0^\infty E(t)t^2dt - \bar{t}^2 = \frac{\int_0^\infty t^2cdt}{\int_0^\infty cdt} - \bar{t}^2 \approx \frac{\sum_i t_i^2 c_i \Delta t_i}{\sum_i c_i \Delta t_i} - \bar{t}^2. \quad (4)$$

The variance, with units of (time)^2, corresponds to the square of the width of the distribution. Additionally, this tracer information is used to obtain flow models, which predict the performance of the real flow reactor.

Figure 15 shows the E-function vs. the dimensionless time $\theta = t/\bar{t}$ for an injected pulse of 0.05 ml of argon in nitrogen as carrier gas. The total volumetric flow rate was 8 ml min^{-1}. The level of dispersion is high as shown by the non-symmetrical shape of the curve. The calculated Pe number for this case was 14. At higher flow rates the Pe was also increasing, approaching to the case were small deviations from plug flow can be assumed [30].

Plug flow model. The plug flow assumption is used as elements of the fluid that enters the vessel at the same moment move through it with constant and equal velocity on parallel paths and leave at the same moment [32]. The concept of plug flow implies that there is no axial mixing in the vessel, but complete radial mixing prevails in a cylindrical vessel. As a consequence, all fluid elements have the same residence time. On the other hand, complete radial mixing implies that fluid properties are uniform across any plane perpendicular to flow direction [33]. Equation (5) represents an ideal dynamic plug flow model,

$$\frac{\partial c_i}{\partial t} = \frac{\partial \dot{n}_i}{A\,\partial l} . \quad (5)$$

For a constant volumetric flow rate,

$$\frac{\partial \dot{n}_i}{A\,\partial l} = \frac{w}{AL}\frac{\partial c_i}{\partial z} , \quad (6)$$

where L/w represents the mean residence time ($\bar{t}$) and z is the dimensionless length coordinate.

Axial dispersion model. The axial dispersion model can be used to describe intermediate cases between complete backmixing and plug flow. There are several cases, in which the deviation from plug flow is not too large and the RTD observed is symmetrical and approaches the Gaussian distribution curve [34]. The axial dispersion model can be considered as the result of a plug flow with a superposition of longitudinal dispersion, where the axial dispersion coefficient D (m^2 s^{-1}) represents the spreading process [30] as illustrated by Fig. 16 for an arbitrary component (i).

The differential equation describing the dispersion model can be expressed by an equation similar to Fick's law for molecular diffusion,

$$N_i = -D\frac{\partial c_i}{\partial l} . \quad (7)$$

For a cylindrical tube, the mass balance of an inert component in a volume element is given by

$$\dot{n}_{i,\text{in}} + \left[\left(-D\frac{\partial c_i}{\partial l}\right)A\right]_{\text{in}} = \dot{n}_{i,out} + \left[\left(-D\frac{\partial c_i}{\partial l}\right)A\right]_{\text{out}} + \frac{\partial \dot{n}_i}{\partial t}. \quad (8)$$

With the relationships

$$\Delta\left(D\frac{\partial c_i}{\partial l}\right)A = \Delta\dot{n}_i + A\Delta l\frac{\partial c_i}{\partial t} ,$$

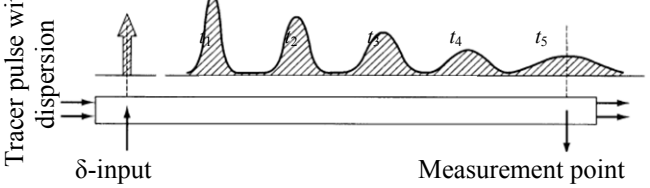

Fig. 16. Spreading process in the dispersion model: pulse propagation.

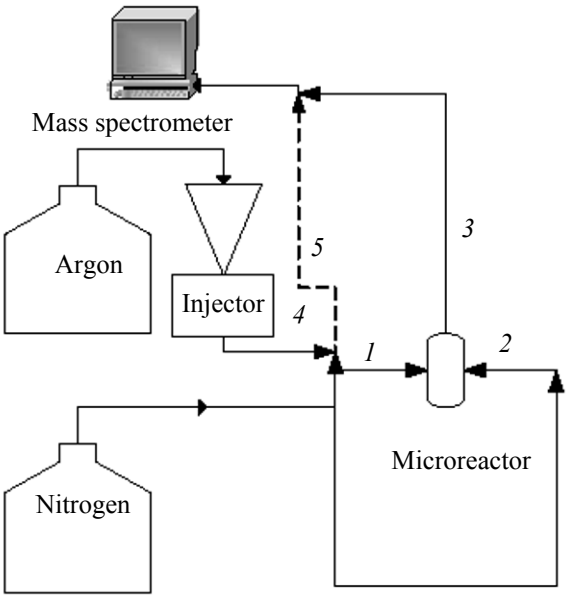

Fig. 17. System used for pulse experiments.

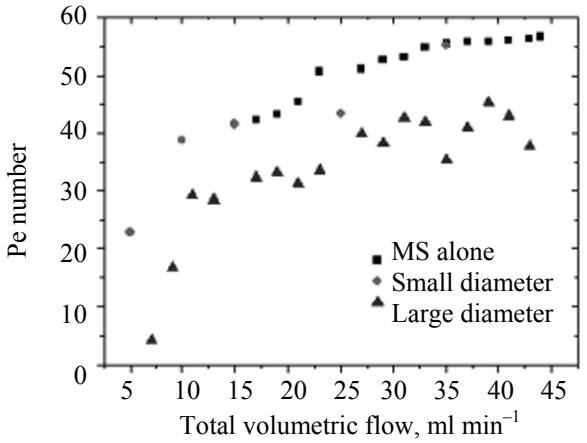

Fig. 18. Degree of dispersion inside the microchannels and mass spectrometer vs. volumetric flow (injected argon pulses in nitrogen as a carrier gas).

Equation (8) can be expressed as

$$\frac{\partial c_i}{\partial t} = \frac{1}{A}\frac{\partial \dot{n}_i}{\partial l} + D\,\frac{\partial^2 c_i}{\partial l^2}. \qquad (9)$$

When the dispersion coefficient is zero, and with $Adl = dV$, the equation of an ideal plug flow reactor is obtained [Eq. (5)].

For a constant volumetric flow rate it follows that $d\dot{n}_i/dl = Vdc_i/dl$. After expressing everything in dimensionless quantities where $z = l/L$, and $w = V/t$, Eq. (10) is obtained:

$$\frac{\partial c_i}{\bar{t}\partial\theta} = -\frac{w}{L}\frac{\partial c_i}{\partial z} + \frac{D}{L^2}\frac{\partial^2 c_i}{\partial z^2}. \qquad (10)$$

which can be rearranged to

$$\frac{\partial c_i}{\partial\theta} = \frac{\partial c_i}{\partial z} + \frac{D}{wL}\frac{\partial^2 c_i}{\partial z^2}. \qquad (11)$$

At this point, it is necessary to introduce the dimensionless Peclet number Pe, which characterizes the degree of dispersion,

$$\mathrm{Pe} = \frac{wL}{D}. \qquad (12)$$

If Pe→∞, axial dispersion is negligible, hence plug flow is obtained. On the other hand, if Pe→0 (D tends to infinity), a large degree of dispersion is present, hence, complete backmixing is approached.

By recording the shape of the tracer curve as it passes the exit of the vessel, it is possible to evaluate the Peclet number by knowing the mean residence time ($\bar{t}$) and the variance (σ^2). The data presented in Fig. 15 are evaluated and the degree of dispersion is calculated. For closed vessels and large deviation from plug flow, Eq. (13) represents the relationship between the variance and the Peclet number:

$$\sigma^2 = \frac{2}{\mathrm{Pe}} - \frac{2}{\mathrm{Pe}^2}\,(1 - e^{-\mathrm{Pe}}). \qquad (13)$$

As just a small deviation from plug flow is obtained, i.e., 1/Pe < 0.01, the tracer curve is narrow and therefore passes the measuring point quickly compared to $\bar{t}$. Hence, the curve is symmetrical and Gaussian in a way that the spread of the curve depends on Pe [30].

In the case where the curve becomes unsymmetrical, i.e., 1/Pe > 0.01, the flow conditions at the inlet and outlet of the vessel (boundary conditions) influence the shape of the concentration curve. Here, various boundary conditions can be considered, such as closed–closed vessels and open–open vessels. For a closed–closed boundary, also known as Danckwerts boundary conditions, it is understood that there is plug flow outside the vessel up to the boundary. In contrast, open-open boundary implies that the flow is undisturbed as it passes the boundary [30].

In order to experimentally measure RTD, as well as to determine the dispersion in the microreactor, pulses of argon were injected using nitrogen as a carrier gas. Figure 17 corresponds to the pulse experiments set up. The nitrogen feed was introduced through the inlets of the microreactor (Fig. 17, positions *1* and *2*), and the

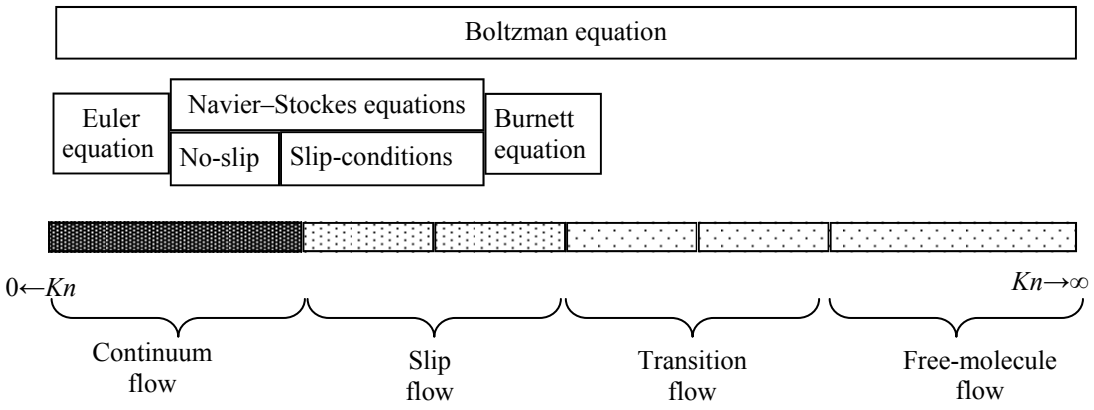

Fig. 19. Knudsen number regimes [37].

pulse of the tracer was further injected by using a six-way valve and a thin tube (Ø 0.5 mm) directly inserted in the microreactor chamber (position *4*). A quadrupole mass spectrometer (Balzers Omnistar GSD 300 O) was connected to the outlet of the microreactor with the purpose of acquiring the response curve from the outlet of the microreactor (position *3*) or the pulse directly, bypassing the microreactor (position *5*). The argon flow was varied from 15 to 50 ml min^{-1}, and the N_2 pulse was of 0.05 ml.

Figure 18 shows the calculated Peclet number inside the microchannels for different tube diameters and for the mass spectrometer (MS) alone. The smaller diameters reduce the dispersion on the system (the Pe number becomes larger) approaching the plug flow behavior (Fig. 18). It was shown that when the reac-tor was bypassed and the pulses were directly fed into the MS, the degree of dispersion was still considerable, indicating that the MS line was accounted for most of the dispersion present on the system.

Computational fluid dynamics. Computational fluid dynamics (CFD), as one of the branches of fluid dynamics, uses numerical methods and algorithms to solve and analyze problems involving fluid flows. CFD is a sophisticated computationally-based design and analysis technique. It gives the possibility of simulating flows of gases and liquids, heat and mass transfer, and chemical reactions, among others. The fundamental bases of any CFD problem are the Navier-Stokes equations, which define any single-phase fluid flow.

Computational fluid dynamics is broadly used for the understanding of microreactor flows as well as a tool for design and efficiency improvement [35]. Furthermore, it can be used to describe the major performance characteristics quantitatively, including, for instance, the mixing efficiency and the residence time behavior of microstructured reactors and mixers. In order to characterize the residence time distribution of microfluid components, dedicated measuring methods as well as mathematical modeling tools are under development to demonstrate the interaction between fluid channel structures and residence time characteristics [36]. Since the flow in microreactors is usually laminar due to the small diameters of the channels, a very tight control over the residence time distribution can be achieved, so that the reactor conditions are well understood [35].

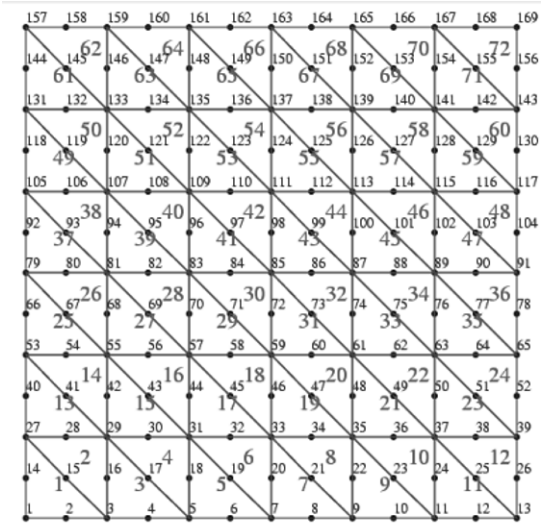

Fig. 20. Example of the FEM grid formulation.

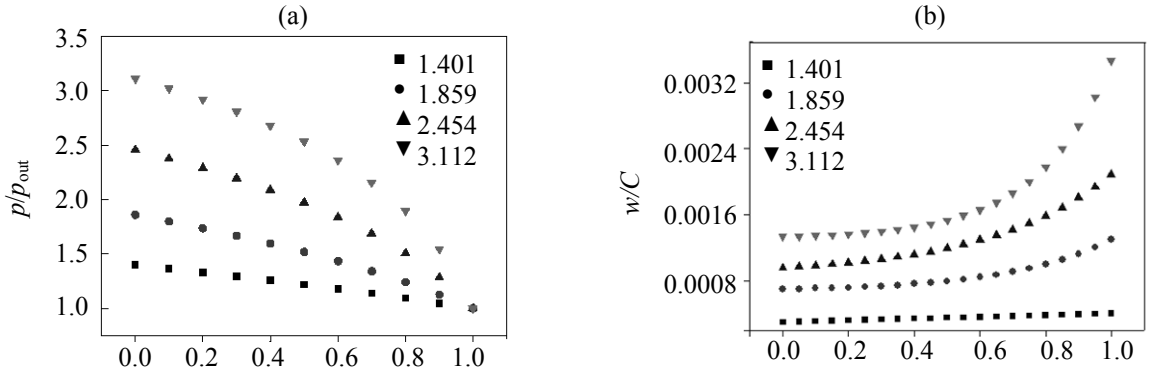

Fig. 21. (a) Normalized modelled pressure and (b) velocity profiles in a microchannel.

An important criterion for characterizing the type of flow is given by the Knudsen number $Kn = \lambda/L$, where l represents the free path of the gas molecules and L is the characteristic length (diameter of the microchannel in our case). The molecules free path is dependent on temperature, pressure and particle diameters and can be calculated as $\lambda = k_B T/\sqrt{2}pd^2$, where k_B is the Boltzmann constant. At the experimental conditions of this work, the Knudsen number has values smaller than 10^{-3}, allowing utilization of the typical Navier-Stokes equations valid for macro flows [Eqs. (14) and (15)]. Figure 19 shows the Knudsen number regimes for different values [37]. The Navier-Stokes equations are in our case given by,

$$\rho\left(\frac{\partial u_i}{\partial t} + u_j\frac{\partial u_i}{\partial x_j}\right) = -\frac{\partial p}{\partial x_i} + \rho g_i + \frac{\partial p}{dx_k}\left[\mu\left(\frac{\partial u_i}{\partial x_k} - \frac{2}{3}\delta_{ik}\frac{\partial u_j}{\partial x_j}\right)\right], \quad (14)$$

$$\frac{\partial \rho}{dt} + \frac{\partial}{dx_i}(\rho u_i) = 0. \quad (15)$$

Equation (14) gives the velocity profiles of the fluid (being the left hand side of the equation the convection term and the right hand side representing the pressure difference, gravity term and viscous dissipation term, in that order), whereas Eq. (15) stands for the mass conservation balance for non-reactive flows. The system consists of four unknowns and four equations.

The equations are a set of coupled differential equations and could, in theory, be solved for a given flow problem by using the methods known from calculus. Instead, a finite element method (FEM) was used. The FEM is a good choice for solving partial differential equations (PDEs). The PDEs were converted into equivalent ordinary differential equations, which are then solved using standard techniques, such as finite differences. The microchannel was divided in a 2D grid (Fig. 20). Each point is surrounded by four neighbouring nodes for the approximation of the derivatives and the problem was solved for density and pressure. Implicit time steps and Newton-Raphson iteration were used for convergence. When the residual of the velocity vector for two successive iterations was less than a defined tolerance (10^{-3}) and the computation was regarded as completed, the values were used. Figure 21 shows the pressure and velocity profiles along the axial direction in a microchannel. Since the microreactor works isothermally, the density is directly proportional to the pressure, with a negative gradient along the channel (Fig. 21a). For preserving the continuity [Eq. (15)], the velocity shows the corresponding increase (Fig. 21b). The effect is most prominent at higher p/p_{out} ratios, where the pressure could drop more than three times [38].

Another alternative for solving the Navier-Stokes equations is computational fluid dynamics. Recently, high speed computers have been used to solve approximations to the equations by using a variety of techniques such as finite difference, finite volume, finite element, and spectral methods.

The commercially available software COMSOL Multiphysics 3.4a was used to simulate the non-reactive flow profile inside the microchannels. Figure 22 shows a SEM micrograph of one channel with its dimensions. Figure 23 presents the mesh used for the simulation of a simple microplate, which consisted in 2300 elements. The physical properties of helium were used for the simulations. Figure 24 presents the velocity profile in the microplate for a total flow of

50 ml min^{-1} calculated with CFD. The prediction of the velocity profile implies that the velocity becomes zero close to the wall (non-slip condition), while it attains a maximum at the centre of the plates. This behavior could easily be extended to a single microplate, expecting the same flow pattern in the microchannel. Additionally, the channel proves to be "long" enough to fully develop the laminar velocity profile for the used flow rate. For smaller flow rates, the residence time increases although the velocity distribution remains similar, i.e., the length of the microchannel allows the development of the flow. Working with lower residence times (higher volumetric flows) assures that the microreactor is operating under the kinetic regime, an important feature when studying the kinetics of reacting flows [38].

A different approach is presented in Fig. 25. Assuming that the velocities in the inlet become slightly larger on the central channels compared to the external ones, the CFD simulations still suggest that after a short time in the microchannel (axial distance ~3 mm), the flow develops completely and the pressure drop in the channels becomes less prominent (Fig. 25), according to the conservation equation [Eq. (15)].

Reactive Flow Modeling

Laminar flow model with radial diffusion. When a chemical reaction is introduced in the system, the equations presented so far have to be modified. Microreactors are known for their fast mass transfer capabilities due to the short diffusion distances. However, it has been stated that despite smaller thickness of the catalytic washcoating, internal diffusion limitations might appear, since the reaction rates are high. Moreover, mass transfer limitations from the gas phase to the catalytic surface are also possible mainly via molecular diffusion if the flow velocity is low [39]. When studying reacting flows through microchannels, the traditional approach has been to assume wall-catalyzed reactions. However, as a porous medium acts as a catalyst (being the advantage its higher surface area, thus higher concentration of active sites) the mathematical problem becomes a fully coupled system of equations of reaction, convection and diffusion, which are challenging to solve numerically [36]. Gobby et al. [40] have developed a model that allows a rapid calculation of some microreacting flows.

Nevertheless, the mathematical problem of generalizing the mass balance in a microchannel and

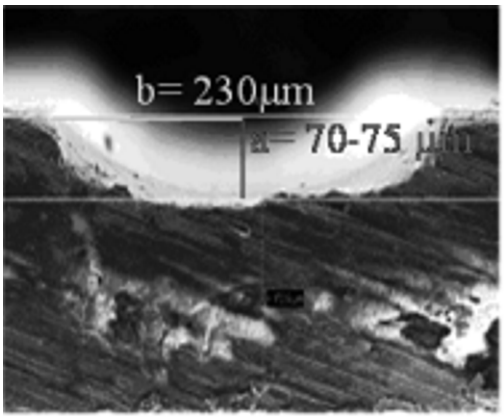

Fig. 22. SEM micrograph of a microchannel with its dimensions.

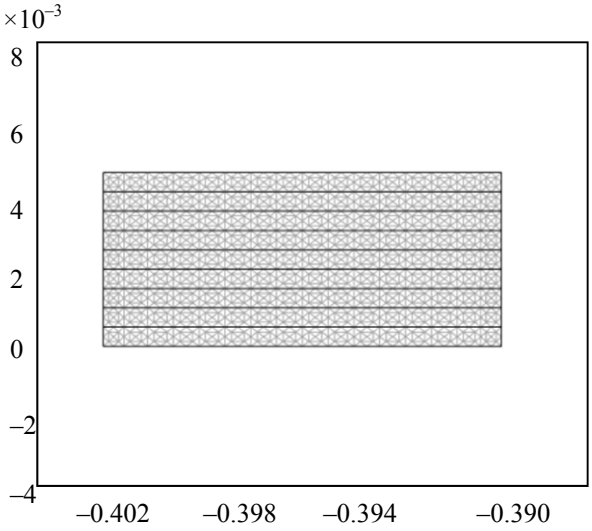

Fig. 23. Mesh used for the CFD simulations.

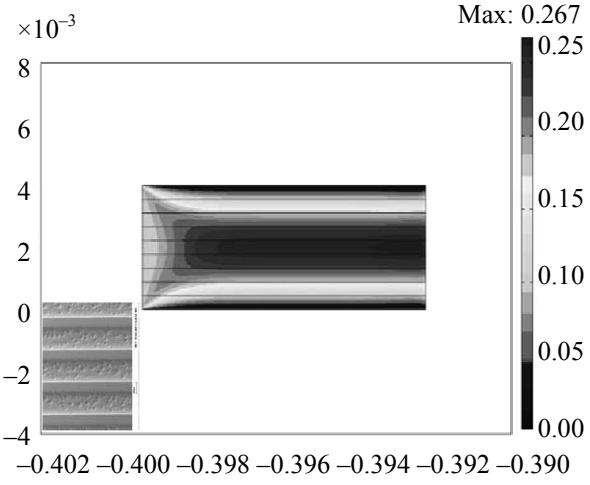

Fig. 24. CFD simulations of an inert flow on a single microplate (50 ml min^{-1}).

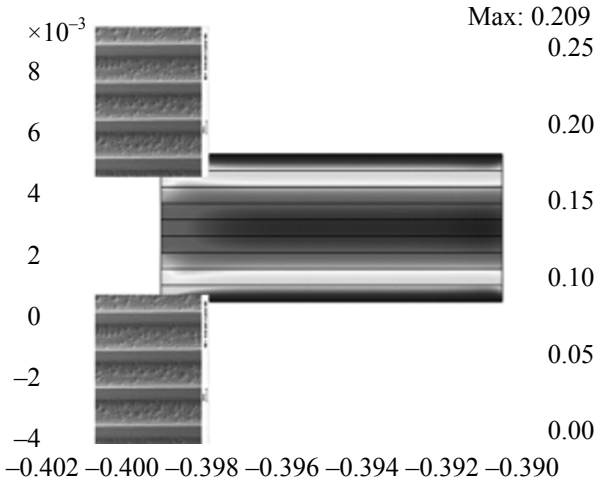

Fig. 25. CFD simulations of an inert flow on a single microplate (50 ml min^{-1}, different inlet velocities, linearly increasing from the outer channels to the center).

its catalytic layer solving the fully coupled problem of chemical reactions with a laminar flow model including radial diffusion and diffusion in the catalyst layer is still to be addressed.

Coupling of the component mass balances of the catalytic layer with the ones in the microchannel was done. The first approach is a pseudo-homogeneous plug flow model. In the case where diffusion limitations appear in the catalytic layer, the model becomes heterogeneous as follows [Eq. (16)]:

$$\varepsilon_p \frac{\partial c_i'}{\partial t} = r_i \rho_p + \frac{D_e}{\delta^2}\left(\frac{\partial^2 c_i'}{\partial x^2} + \frac{s}{x}\frac{\partial c_i'}{\partial x}\right), s \in [0,2] \text{ and } s \in [0,1], \quad (16)$$

where the thickness of the catalytic layer (δ) varies along the microchannel.

The mass balance in the microchannel with radial diffusion is given by

$$\frac{\partial c_i(r, l)}{\partial t} = D_{M,i}\left[\frac{\partial^2 c_i(r, l)}{\partial r^2} + \frac{\partial c_i(r, l)}{\partial r}\right] - \frac{\partial [c_i(r, l) w(r)]}{\partial l}, \quad (17)$$

$$w(r) = 2\overline{w}\left[1 - \left(\frac{r}{R}\right)\right],$$

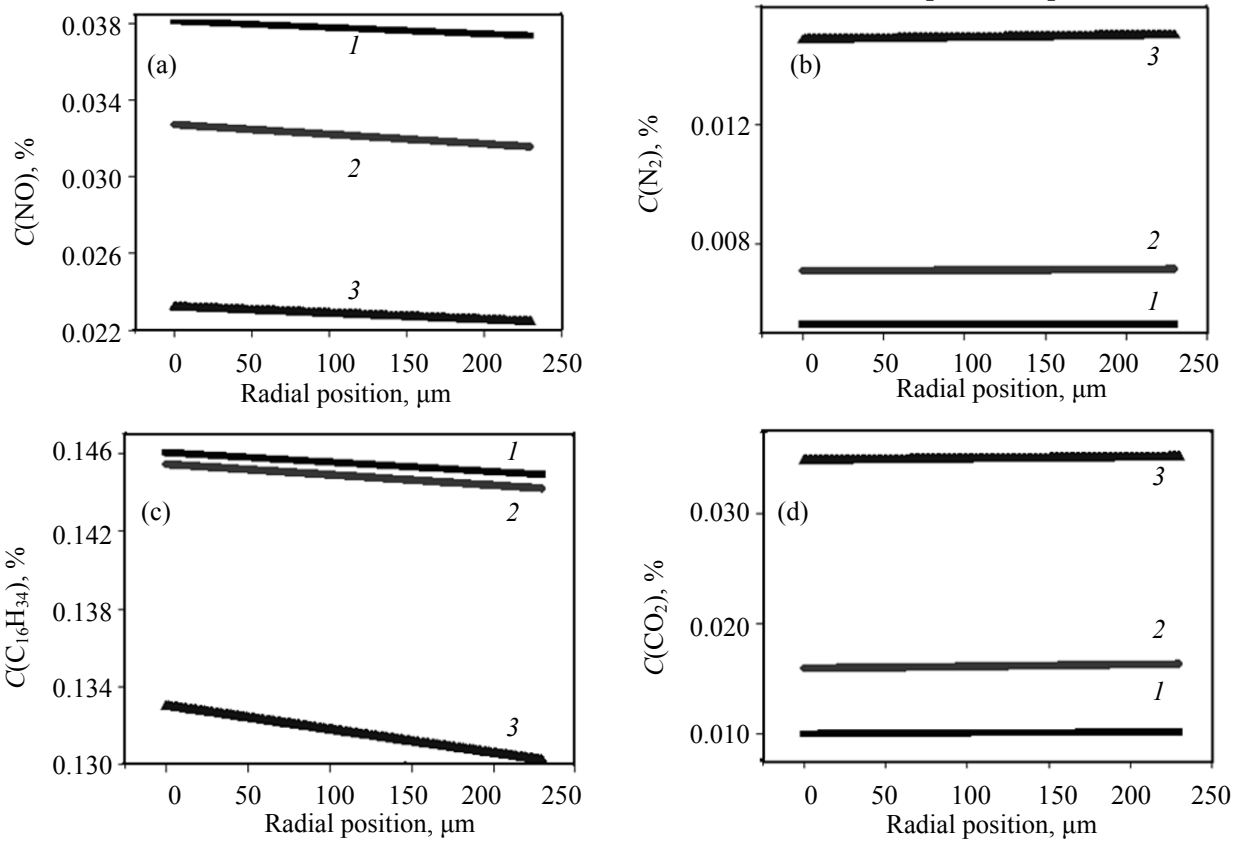

Fig. 26. Radial concentration profiles of the microchannel at different axial positions for (a) NO, (b) N_2, (c) $C_{16}H_{34}$, and (d) CO_2.

which has the boundary conditions

$$\frac{\partial c_i}{\partial r} = 0,\ r = 0, \quad \frac{D_e}{\delta}\left(\frac{\partial c_i'}{\partial r}\right)_{r=R},$$

$$\left(\frac{\partial c_i'}{\partial x}\right)_{x=1} = 0.$$

For the sake of simplicity, the microchannels were approximated to have a circular geometry [Eq. (17)]. A distribution function $E(\delta)$ as a function of the above-mentioned thickness δ can be obtained as well; hence

$$\frac{D_e}{\delta}\left(\frac{\partial c_i'}{\partial x}\right)_{x=0}$$

can be substituted by, so

$$D_e \int_{\delta_{min}}^{\delta_{max}} E(\delta)\left(\frac{\partial c_i'}{\partial x_\delta}\right)_{x_\delta=0} \partial\delta.$$

Equation (16) is to be solved for various wall thickness (δ).

Kinetic modeling. According to Schouten et al. [41] the following steps can be distinguished in the determination of kinetic equations: (1) determination of reaction rates at varying operating conditions; (2) development of a mathematical model for the kinetic reactor; (3) development of a number of possible reaction rate expressions; (4) determination of parameter values in a kinetic model on the basis of the experiments; and (5) choice of the best kinetic model.

A very precise chemical analysis is necessary for catalyst testing and kinetic measurements, particularly in connection of microreactors, since the gas amounts are typically small. In addition, even trace amounts of by-products must be analyzed very carefully. Based on chemical knowledge and experimental results, hypotheses on the reaction mechanisms can be made and based on such hypotheses, the rate equations for the process can be derived. Depending on the case, quasi-steady state or quasi-equilibrium approximations can be used to simplify the rate equations. The rate equations can further be implemented in a reactor simulation and parameter estimation software, where a library of reactor models, numerical solvers for differential equations as well as parameter estimation software are available. The parameter estimation software Modest 6.0 is capable of handling these types of tasks [42]. After the parameter estimation, the quality of the kinetic parameters may be checked with statistical methods, and physical considerations can be taken to confirm that the kinetic parameters (rate constants and adsorption parameters) are physically meaningful. The two mentioned examples will be discussed below, HC-SCR of NO_x (Case a) and formation of ethylene oxide (Case b) in a gas-phase microreactor.

Case a: Detailed Kinetic Modeling of SCR in Microreactor

Kinetic parameters for the HC-SCR of NO_x over different catalysts have been investigated in [43, 44]. However, kinetic studies for biodiesels are very scarce, and kinetic data are desirable for design and optimization of engines and exhaust-gas treatment systems. We used hexadecane, a model component for second generation biodiesel and a fuel with excellent properties [45]. By systematically varying the concentrations NO, O_2 and $C_{16}H_{34}$, the reaction orders as well as kinetic parameters of the proposed mechanism were calculated. Concentrations of 500–2000 ppm NO, 188–468 ppm hexadecane, and 3–15 vol % O_2 were used, keeping helium as a balance gas. The concentration of H_2O was kept constant at 12 vol %. The results were treated to obtain the reaction orders with respect to NO, $C_{16}H_{34}$ and O_2 [46].

Two important reactions in the SCR were found to be as follows: $2NO + C_{16}H_{34} + 23.5O_2 \rightarrow N_2 + 16CO_2 + 17H_2O$; and $C_{16}H_{34} + 24.5O_2 \rightarrow 16CO_2 + 17H_2O$. The multi-step mechanism of simple chemical transformations, as well as the overall reactions are summarized in Table 2 and extensively discussed in [47].

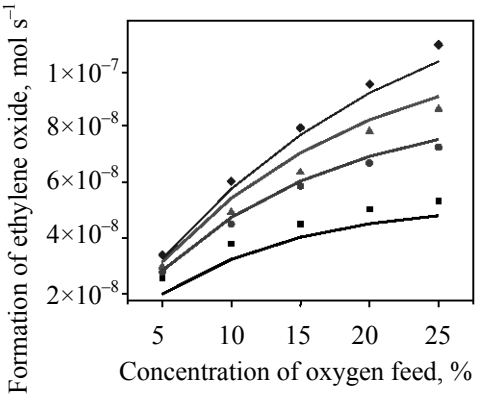

Fig. 27. (Symbols) Experimental and (lines) predicted rates of ethylene oxide formation at different ethylene oxide concentrations over pure silver microchannels. Reaction conditions: (■) 5 vol % ethylene; (●)10 vol % ethylene; (▲)15 vol % ethylene; and (♦) 25 vol % ethylene; total flow 6 $cm^3\ min^{-1}$ at 260°C.

An example of the development of the kinetic model is provided here. The total number of reaction routes was determined by the expression proposed by Horiuti and further developed by Temkin [48]. The concentrations of the adsorbed intermediates were expressed as surface coverages (θ_i), according to the ideal case of chemisorption on surface reactions, developed by Langmuir [49]. The quasi-equilibrium approximation was assumed for the adsorption of the reactants [Eqs. (18)–(21)]:

$$2NO + C_{16}H_{34} + 23.5O_2 \rightarrow N2 + 16CO_2 + 17H_2O,$$

$$C_{16}H_{34} + 24.5O_2 \rightarrow 16CO_2 + 17H_2O.$$

$$\theta_{NO} = K_1 c_{NO} \theta_v, \quad (18)$$

$$\theta_O = \sqrt{K_3 c(O_2) \theta_v}, \quad (19)$$

$$\theta_{CO} = K_6 c_{CO} \theta_v, \quad (20)$$

$$\theta(NO_2) = K_{15} c(NO_2) \theta_v, \quad (21)$$

where K_i represents the equilibrium constants of each species. The formation of NO_2 was observed when hexadecane was applied as a reducing agent, contrary to the case when octane was used [39], hence, it was included in the mechanism. When deriving the equations, the concentrations of surface intermediates were assumed to be in the steady state, meaning that the sum of the rates of formation of surface

Table 2. Proposed mechanism and routes of the $C_{16}H_{34}$-SCR of NO over Ag/Al_2O_3-coated microchannels [47]

Step	Reaction	$N^{(1)}$	$N^{(2)}$	$N^{(3)}$	$N^{(4)}$	$N^{(5)}$	$N^{(6)}$	$N^{(7)}$	$N^{(8)}$	$N^{(9)}$
1	$NO + * \leftrightarrow NO*$	0	0	1	1	1	1	0	1	1
2	$NO* + * \rightarrow N* + O*$	0	0	0	0	0	0	0	-1	0.5
3	$O_2 + 2* \leftrightarrow 2O*$	49	33	24	16	23	15	0.5	0.5	0
4	$2N* \rightarrow N_2 + 2*$	0	0	0	0	0	0	0	-1	0
5	$NO* + O* \rightarrow NO_2 + 2*$	0	0	0	0	0	0	0	1	0
6	$CO + * \leftrightarrow CO*$	0	-32	0	-16	0	-16	1	0	1
7	$CO* + O* \rightarrow CO_2 + 2*$	32	0	16	0	16	0	1	0	0.5
8	$C_{16}H_{34} + O* + * \rightarrow C_{16}H_{33}* + OH*$	2	2	1	1	1	1	0	0	0
9	$C_{16}H_{33}* + NO* \rightarrow C_{16}H_{33}NO* + *$	0	0	1	1	0	0	0	0	0
10	$2C_{16}H_{33}NO* \rightarrow N_2 + 2C_{16}H_{33}O*$	0	0	0.5	0.5	0	0	0	0	0
11	$C_{16}H_{33}O* + 48O* \rightarrow 16CO* + 33OH*$	2	2	1	1	1	1	0	0	0
12	$C_{16}H_{33}* + O* \rightarrow C_{16}H_{33}O* + *$	2	2	0	0	0	0	0	0	0
13	$2OH* \rightarrow H_2O + O*$	34	34	17	17	17	17	0	0	0
14	$C_{16}H_{33}NO* + NO* \rightarrow N_2 + C_{16}H_{33}O* + O*$	0	0	0	0	1	1	0	0	0
15	$NO_2 + * \leftrightarrow NO_2*$	0	0	0	0	1	1	0	0	0
16	$C_{16}H_{33}* + NO_2* \rightarrow C_{16}H_{33}NO* + O*$	0	0	0	0	1	1	0	0	0
17	$N* + CO* \rightarrow NCO* + O*$	0	0	0	0	0	0	0	0	0.5
18	$NCO* + H_2O \rightarrow NH_2* + CO_2$	0	0	0	0	0	0	0	0	0.5
19	$NH_2* + NO* \rightarrow N_2 + H_2O*$	0	0	0	0	0	0	0	0	0.5
20	$N* + NO* \rightarrow N_2O* + *$	0	0	0	0	0	0	0	1	0
21	$N_2O* \rightarrow N_2 + O*$	0	0	0	0	0	0	0	1	0

$N^{(1)}$:
$2C_{16}H_{34} + 49O_2 \rightarrow 32CO_2 + 34H_2O$

$N^{(2)}$:
$2C_{16}H_{34} + 33O_2 \rightarrow 32CO_2 + 34H_2O$

$N^{(3)}$:
$C_{16}H_{34} + NO + 24O_2 \rightarrow 16CO_2 + 17H_2O + 0.5N_2$

$N^{(4)}$:
$C_{16}H_{34} + NO + 16O_2 \rightarrow 16CO + 17H_2O + 0.5N_2$

$N^{(5)}$:
$C_{16}H_{34} + NO + NO_2 + 23O_2 \rightarrow 16CO_2 + 17H_2O + N_2$

$N^{(6)}$:
$C_{16}H_{34} + NO + NO_2 + 15O_2 \rightarrow 16CO + 17H_2O + N_2$

$N^{(7)}$:
$CO + 0.5O_2 \rightarrow CO_2$

$N^{(8)}$:
$NO + 0.5O_2 \rightarrow NO_2$

$N^{(9)}$:
$NO + CO \rightarrow 0.5N_2 + CO_2$

intermediates in elementary reactions is equal to the sum of the rates of its consumption in other elementary steps.

For instance, for $C_{16}H_{33}$* it follows that

$$r_8 = r_9 + r_{12} + r_{16}. \quad (22)$$

Substituting each corresponding rate expressions (from Table 2) in Eq. (22) yields

$$k_8 c_{hex}\theta_O = k_9 c_{hex}\theta_{NO} + k_{12} c_{hex}\theta_O + k_{16} c_{hex}\theta_{NO}. \quad (23)$$

Solving for θ_{hex}, and introducing Eqs. (18), (19), and (21), an expression for the hexadecane coverage ($C_{16}H_{33}$*) is obtained:

$$\theta_{hex} = \frac{k_8 c_{hex}\sqrt{K_3 c(O_2)}}{k_9 K_1 c_{NO} + k_{12}\sqrt{K_3 c(O_2)} + k_{16} K_{15} c(NO_2)}\,\theta_v. \quad (24)$$

Following the same procedure, coverages for other species could be obtained. In the cases where more than one solution was possible (quadratic expressions), the only solution with physical meaning was considered ($0 < \theta < 1$).

When calculating reaction orders of NO for NO reduction, their value was found to be between 0.6–0.9 at all temperature range (250–550ºC). The apparent reaction orders for hexadecane were increasing from zero at lower temperatures (200ºC) until 1.23 at 550ºC. Additionally, the orders with respect to $C_{16}H_{34}$ seem to be higher than the orders of NO, which indicates the hydrocarbon reactivity dominates the rate of NO_x reduction [46].

Kinetic studies combined with mathematical modeling are a powerful tool for better understanding and obtaining a deeper insight into catalysis and the mechanisms of chemical processes. The kinetic modeling and parameter estimation performed in this work were based on the experimental data attained in the activity tests. Isothermal plug flow model was used to describe the mass balance in the microchannels. The kinetic data were simultaneously fitted by non-linear regression to the rate equations as a function of the independent variables: concentrations of hexadecane, NO, NO_2, CO, CO_2, water and oxygen. The model predictions and kinetic parameters were obtained by using ModEst 6.0 [42]. The estimated parameters are presented, as well, in [47].

Equations (16) and (17) are to be used when laminarity of the flow is expected. In microreactors, it is very common to have laminar flow inside the channels. The dynamic model consisting of a system of partial differential equations can be discretized using a finite differences formulation with respect to the spatial coordinate. We have used the same HC-SCR system for testing the validity of the model. The resulted ordinary differential equations were solved with an appropriate method for stiff differential equations, e.g., backward differences to guarantee stability and convergence. The concentration profiles at different axial positions for reactants (NO and $C_{16}H_{34}$) and products (N_2 and CO_2) are shown in Fig. 26 [38].

The concentration gradient was found to be rather small, indicating that the mass transfer limitations are indeed negligible. Closer to the reactor outlet (normalized length l = 0.9), the concentration gradient between the bulk phase and the catalytic layer was slightly larger than at shorter axial distances (l 0.1 and l 0.2). However, the changes of the radial concentration profiles resulted minimal, demonstrating the accuracy of using a plug flow model for representing the catalytic behavior of the microchannel for this particular chemical system. For cases of faster reaction, it is expected a more pronounced profile inside the microchannels.

Assuming that the diffusion from the bulk phase to the solid film (external mass transfer) is slower than the intra-catalytic layer mass transfer (internal), since the diffusion path from the bulk to the catalytic layer is much larger then the intra-layer one, the internal mass transfer was considered to be minor. In general, the model described very well the behavior of gas-phase SCR of NO_x over Ag/alumina microchannels.

Case b: Detailed Kinetic Modeling of Ethylene Oxide Production in a Microreactor

The kinetics of ethylene epoxidation and combustion have been studied extensively by a number of authors. Moreover, no single kinetic expression that reproduces the kinetics for both ethylene-rich and oxygen-rich feeds exists. Instead, different kinetic expressions are used for different reaction conditions. This indicates a very complicated kinetics for this process. The most favoured kinetic expressions in the literature seem to be of competitive Langmuir–Hinshelwood type [50].

For the kinetic runs, the catalyst was first treated with ethylene in order to remove most of the adsorbed oxygen from the catalyst after the previous experiment and further outgassed with oxygen in order to achieve stability, even if the conversions were lower. Overall, a

good stability and activity of the catalyst was achieved and a set of kinetic runs were completed with pure silver plates.

Since the characteristic lengths in microreactors and the high surface-to-volume ratio, heat and mass transfer effects tend to be very high; hence, kinetic regime is easily achievable. The temperature for the experiments was kept constant at 260°C and the total flow was set to 6 cm^3 min^{-1} for all the experiments (residence times 0.138 s). A total of 25 experiments were conducted with varying the ethylene and oxygen concentration from 5 vol % to 25 vol %.

Petrov et al. [51] investigated steady-state kinetics of ethylene epoxidation over $Ag/\gamma\text{-}Al_2O_3$ catalyst promoted by Ca additive in a circulation flow system. Their empirical kinetic model corresponds to a single site Eley–Rideal mechanism, where adsorbed molecular oxygen produces ethylene oxide and the atomic oxygen is responsible for the complete oxidation reaction. Both reactions proceed on the same catalytic site. Rate expressions were given to partial and complete oxidation reactions. Nonetheless, in later studies [52, 53] the Eley–Rideal type expressions were rejected as contradiction to their experimental observations.

Borman and Westerterp [53] studied oxidation of ethane with industrial $Ag/\gamma\text{-}Al_2O_3$ catalyst in an internal recycle reactor. It was found that all reactants and reaction products influence the reaction rates. The reaction rate expression was based on a Langmuir-Hinshelwood mechanism in which adsorbed ethylene and dissociatively adsorbed oxygen react to yield ethylene oxide, carbon dioxide and water. The two reactions are assumed to proceed over different catalytic sites and the surface reactions are rate-limiting. Other studies have also pointed out the importance of the products in the rate expressions [54]. On the other hand, by using a differential reactor and an $Ag/Cs/\gamma\text{-}Al_2O_3$ catalyst Lafarga et al. [52] studied kinetics of the ethylene epoxidation network. In their experimental conditions (temperature range 210–270°C, total pressure 1 bar), both ethylene and oxygen influenced the reaction rates. The influence of the products was found to be negligible due to their low partial pressure in the reactor. In this work, due to the low concentration of products (from 0.03 to 0.30 vol %) compared to concentration of reactants (from 5 to 25 vol %), the influence of products in the model was assumed to be minimal and thus the product inhibition is not accounted for in the kinetic model. The total oxidation reaction of ethylene oxide to carbon dioxide and water was also neglected. The results with kinetic experiments indicated the presence of adsorption terms for both ethylene and oxygen, thus a Langmuir-Hinshelwood mechanism can be assumed for the reaction. The rate-limiting step was assumed to be the surface reaction between adsorbed ethylene and adsorbed oxygen as suggested by many of the recent studies [52–54].

A plug-flow reactor model was used to describe the microreactor. The conversions were low (< 0.30% for kinetic experiments) and hence the concentration and temperature gradients were small. Under the flow conditions, a steady-state plug-flow was approximated. The catalyst was pure silver catalyst, thus the effect of internal diffusion can be assumed to be negligible.

While many studies agree that the reaction is based on the Langmuir–Hinshelwood mechanism, a controversy exists between whether oxygen adsorbs dissociatively or molecularly on the catalytic site. Both models were proposed: the first one assumed competitive adsorption of ethylene and oxygen on the catalyst surface. The oxygen adsorbs dissociatively being the surface reaction the rate-limiting step as presented in Eq. (25).

$$r_1 = \frac{k' c_{\text{ethylene}} \sqrt{c_{\text{O}}}}{\left(1 + K_{\text{ethylene}} c_{\text{ethylene}} \sqrt{K_{\text{O}} c_{\text{O}}}\right)^2} \qquad (25)$$

where r_1 is the rate for conversion of ethylene to ethylene oxide, $k' = kK_{\text{E}}(K_{\text{O}})^{1/2}$, c_i, concentration of compound i, K_i , adsorption constant of compound i, and k, rate constant for ethylene oxide formation.

The second model [Eq. (26)] assumed competitive adsorption of ethylene and molecular oxygen on the surface, while the surface reaction was considered to be the rate-limiting step.

$$r_1 = \frac{k' c_{\text{ethylene}} c_{\text{O}}}{(1 + K_{\text{ethylene}} c_{\text{ethylene}} + K_{\text{O}} c_{\text{O}})^2}. \qquad (26)$$

where r_1 is the rate for conversion of ethylene to ethylene oxide, $k' = kK_{\text{E}}K_{\text{O}}$, c_i, concentration of compound i, K_i, adsorption constant of compound i, and k, rate constant for ethylene oxide formation. Even if the first model resulted in a good fitting (degree of explanation 93%), the second model fitted the experimental data best, obtaining a degree of explanation of 96.7%,

The kinetic modeling and parameter estimation performed in this work are based on the experimental data obtained in the activity experiments. The kinetic data was simultaneously fitted by nonlinear regression to the rate equations as a function of the independent variables: concentrations of C_2H_4 and O_2 that were measured at the inlet and outlet of the microreactor. The model predictions and kinetic parameters were obtained by using the parameter estimation software ModEst 6.0 [41]. A stiff ODE-solver (Odessa) with the Simplex–Levenberg–Marquardt algorithm implemented in the software was used to solve the system. The sum of residual squares was minimized using the following objective function [Eq. (25)]:

$$Q = \|c_{\text{exp}} - c_{\text{est}}\|^2 = \sum_i \sum_i (\text{exp},it - c_{\text{est},it})^2. \quad (27)$$

The degree of explanation that represented the accuracy of the fit was given by:

$$R^2 = 100\times\left(1 - \frac{\|c_{\text{exp}} - c_{\text{est}}\|^2}{\|c_{\text{exp}} - \bar{c}_{\text{exp}}\|^2}\right). \quad (28)$$

where $\bar{c}_{\text{exp}}$ represents the mean value of all the data points. In the model, the temperature dependences of the rate constants were expressed as a typical Arrhenius dependence. The parameters estimated from Model 2 are presented in Table 3.

The comparisons between estimated and experimental values of rate of ethylene oxide formation are shown in Figs. 27 and 28, while the parity plot is presented in Fig. 29.

Table 3. Kinetic parameters obtained from Model 2

Parameter	Value
K_E	132 ± 40.1
K_O	77.4 ± 13.4
k'	$(9.75 \pm 4.42)\times10^{-3}$
k	$(9.54 \pm 5.33)\times10^{-7}$

The increasing oxygen concentration had a positive influence on the formation of ethylene oxide as shown in Fig. 27. For example, at 10 vol % ethylene in feed, the rate of formation increased from 2.8×10^{-8} to 7.2×10^{-8} mol s^{-1}, while oxygen concentration in feed increased from 5 to 25 vol %. The rate of formation increases more rapidly first and start to moderate as higher oxygen concentrations are reached. Similar results of influence of oxygen concentration were observed by Kestenbaum et al. [55] and Lafarga et al. [52].

It was also observed that at higher concentrations of reactants, the rates of formation of ethylene oxide as well as carbon dioxide were enhanced in similar ways. Nonetheless, when increasing the oxygen concentration, the rate of ethylene oxide formation increased more than the rate of formation of carbon dioxide, which leads to a selectivity increase in the reaction. As the ethylene concentration was increased in the feed, the rates of formation of ethylene oxide followed the same trend. However, as high ethylene concentrations

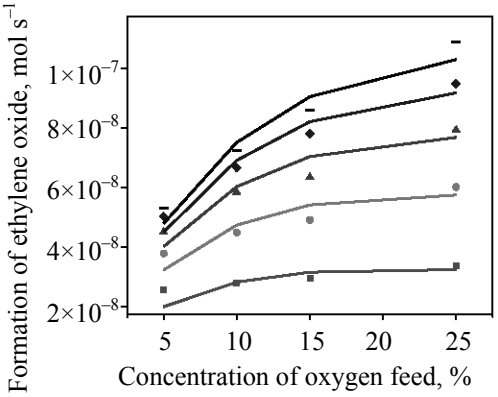

Fig. 28. (Symbols) Experimental and (lines) predicted rates of ethylene oxide formation at different oxygen concentrations over pure silver microchannels. Reaction conditions: (■) 5 vol % oxygen; (●) 10 vol % oxygen; (▲) 15 vol % oxygen; (♦) 20 vol % ethylene; and (-) 25 vol % oxygen; total flow 6 cm^3 min^{-1} at 260°C.

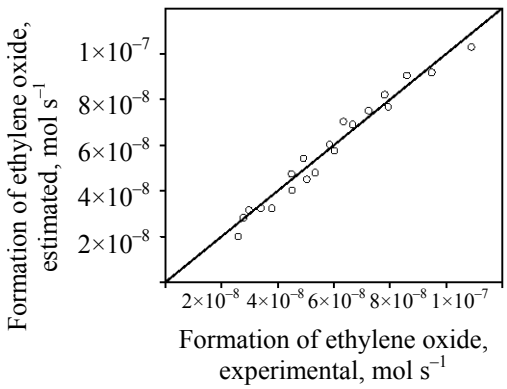

Fig. 29. Parity plot of the fit of the model: experimental vs. estimated rate of formation of ethylene oxide. Degree of explanation 96.7%.

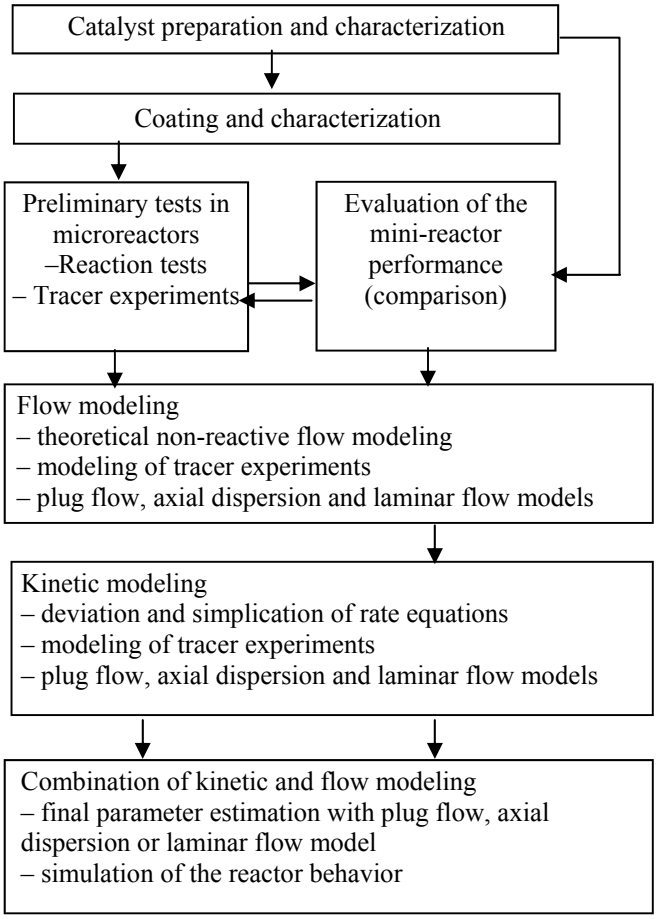

Fig. 30. Proposed approach for the determination of kinetics in gas-phase microreactors.

were reached (above 15 vol %), the rates of formation began to stabilize indicating a possible saturation of catalytic sites (Fig. 28).

In the ethylene epoxidation reaction over silver catalyst, the adsorption of oxygen is arguably the most important aspect of the reaction mechanism. The special selectivity of the silver catalyst in the partial oxidation of ethylene has been attributed to its adsorption characteristics for the oxygen. Three species of oxygen, i.e. the molecular, the atomic and the subsurface oxygen, are generally accepted in the literature [56].

The mechanism of oxygen adsorption (molecular vs. dissociative) still remains controversial. Even if it is true that Model 2, which assumes molecular adsorption of oxygen gave better experimental data fit, a good estimation was also achieved with Model 1 that assumed dissociative adsorption of oxygen. Further studies, e.g., the use of transient techniques and isotope exchange, might be required in order to develop a more precise kinetic model for the partial oxidation of ethylene.

There is a general agreement that the atomic oxygen is the active oxygen species both for ethylene epoxidation and total oxidation, while molecularly adsorbed oxygen is rather inactive [50, 57–58]. Subsurface oxygen is believed to play an important role, as it is necessary for obtaining high selectivity to ethylene oxide, although it does not directly participate in catalytic events. The selectivity to ethylene oxide is governed by the binding state of atomic oxygen, which can exist on the catalyst surface in two extreme conformations. Weakly bound, electrophilic adsorbed oxygen reacts preferentially with the C=C bond of the adsorbed ethylene thus producing ethylene oxide, while the strongly bound ionic oxygen reacts with the hydrogen atoms of the adsorbed ethylene breaking the C–H bond and forming carbon dioxide. This explains the role of subsurface oxygen, the presence of which causes a weakening in the bond strength of adsorbed atomic oxygen via withdrawal of electrons from the silver sites, thus favoring the formation of the electrophilic oxygen atoms [59].

Comparison between the experimental data and calculated values is given in Fig. 29. The proposed model was fitting the data with a very good degree of accuracy (97% degree of explanation). Sometimes, in these types of systems, problems of overparametrization could occur. In order to discard this possibility, sensitivity analysis was applied observing a clear minimum in the objective function (not shown).

SUMMARY

The purpose of this review was to show the versatility of gas-phase microreactors for the determination of kinetics of chemical systems. Precise kinetic models were demonstrated for two industrially-relevant cases: (a) the continuous selective catalytic NO reduction by hydrocarbons in the excess oxygen at 150–550°C; and (b) the catalytic production of ethylene oxide, one of the most important intermediates in the world. Figure 30 shows the summary of the procedure described along the text.

For the HC-SCR case, the in-house impregnated metal/support catalyst on the microchannels showed good activity, compared to that in minireactors in the reduction of NO with hydrocarbons under lean conditions. Still, the intrinsic benefits provided by the

micro-compared with the minireactor present a good alternative for catalytic studies of this kind.

Kinetic parameters of the selective catalytic reduction of NO by using second generation biofuels (hexadecane) were estimated with non-linear regression using simplex and Levenberg–Marquardt algorithms and with the plug flow reactor model. A detailed kinetic scheme was suggested. A mathematical model of laminar flow with radial diffusion and diffusion in the catalytic layer was also developed suggesting that the radial diffusion on the channels was reasonably small for this chemical system.

For the second example, the production of ethylene oxide over pure silver microplates was investigated, obtaining selectivities up to 51%, comparable to values found in the literature. The pure silver plates were further investigated and a kinetic model of the epoxidation reaction was developed. Two models of competitive Langmuir–Hinshelwood type were developed for the partial oxidation of ethylene. The surface reaction between adsorbed ethylene and either molecular or dissociatively adsorbed oxygen was considered the rate-limiting step and a model based on the competitive adsorption of ethylene and molecular oxygen on the surface fitted the experimental data best.

Microreactors are a powerful and versatile tool for the determination of gas-phase kinetics and additionally, they can be implemented in-situ for catalytic abatement of exhaust gases as well as production of intermediates. Microreactors enable an efficient approach to the development of new catalyst materials for gas-phase reactions. The interaction between catalyst preparation, characterization and testing is improved by microreactor technology, since a lot of catalyst modifications can be efficiently screened with microdevices. In future, more attention should be focused on the combination of microanalysis (on-line sensors, spectroscopic methods, micro gas chromatotography) and microreactors technology. An ideal system will consist of a flexible parallel screening microreactor-microanalysis kit, which can be used both for catalyst development and, with some modifications, for on-site production of chemical intermediates.

NOTATION

A = cross-sectional reactor area;

C = speed of sound;

c_i = concentration of species in the bulk phase;

c_i' = concentration of species in the catalyst layer;

d = diameter of the gas particles;

D = dispersion coefficient;

D_e = effective diffusion coefficient;

$D_{M,I}$ = molecular diffusion coefficient;

E = exit age distribution function;

g_i = component i of the gravity;

k_B = Boltzmann constant;

k_j = rate constant for reaction j;

K = equilibrium constant;

Kn = Knudsen number;

l = axial coordinate;

$\dot{n}$ = molar flow;

p = total pressure;

Pe = Peclet number;

R = reactor radius;

r = radial coordinate;

r_i = rate of reaction i;

s = form factor;

t = time;

$\bar{t}$ = mean residence time;

T = temperature;

u_i = component i of the flow velocity;

V = volume;

$w(r)$ = flow velocity in the l direction;

$\bar{w}$ = average flow velocity;

x = radial coordinate along the washcoat depth;

x_i = physical coordinate in the i-direction;

z = dimensionless reactor coordinate ($z = l/L$);

δ = thickness of the catalytic layer

$\delta_{i,k}$ = Kronecker delta ($t/\bar{t}$); $\begin{cases} i = k \to 1 \\ i \neq k \to 0 \end{cases}$

ε_p = porosity of the coating;

θ = dimensionless time;

θ_i = amount of adsorbed species i

μ = dynamic viscosity

ρ = fluid density

ρ_p = density of the catalyst particle

σ = variance.

REFERENCES

1. Ehrfeld, W., Hessel, V., and Löwe, H., *Microreactors – New Technology for Modern Chemistry*, Weinheim: Wiley−VCH, 2000.
2. Hessel, V., Renken, A., Schouten, J.C., and Yoshida, J.-I., *Handbook of Microprocess Technology*, Weinheim: Wiley−VCH, 2009.
3. Jensen, K., *Chem. Eng. Sci.*, 2001, vol. 56, p. 293.
4. deMello, *Nature,* 2006, vol. 442, p. 394.
5. Ajmera, S. K., Delattre, C., Schmidt, M. A., and Jensen, K.F., *Sens. Actuators B: Chem.*, 2002, vol. 82, p. 297.
6. Pieters, B., Andrieux, G., and Eloy, J., *Chem. Eng. Technol*., 2007, vol. 30, p. 407.
7. Walter, St., Malmberg, St., Schmidt, B., and Liauw, M.A., *Catal. Today*, 2005, vol. 110, p. 15.
8. Hogan, J., *Nature,* 2006, vol. 442, p. 27.
9. Kralish, D. and Kreisel, G., *Chem. Eng. Sci.,* 2007, vol. 62, p. 1094.
10. Kiwi-Minsker, L. and Renken, A., *Catal. Today*, 2005, vol. 110, p. 2.
11. Mills, P.L., Quiram, D.J., and Ryley, J.F., *Chem. Eng. Sci*., 2007, vol. 62, p. 6992.
12. Hernández Carucci, J.R., Sosa, J., Arve, K., Karhu, H., Mikkola, J.-P., Eränen, K., Salmi, T., and Murzin, D.Yu., *Catalysis: Principles, Types and Applications*, Nova Publishers, accepted.
13. Hernández Carucci, J.R., Halonen, V., Eränen, K., Wärnå, J., Ojala, S., Huuhtanen, M., Keiski, R., and Salmi, T., *Ind. Eng. Chem. Res*., 2010, vol. 49, p. 10897.
14. Howell, R.S. and Hatalis, M.K., *J. Electrochem. Soc*., 2002, vol. 149, p. 143.
15. Sebastián, V., de la Iglesia, O., Mallada, R., Casado, L., Kolb, G., Hessel, V., and Santamaría, J., *Microporous Mesoporous Mater*., 2008, vol. 115, p. 147.
16. Moulder, J.F., Stickle, W.F., Sobol, P.E., and Bomben, K.D., *Handbook of X-ray Photoelectron Spectroscopy, Perkin Elmer Corp.*, Physical Electronics Division, USA, 1992.
17. Klingstedt, F., Eränen, K., Lindfors, L.-E., Andersson, S., Cider, L., Landberg, C., Jobson, E., Eriksson, L., Ilkenhans, T., and Webster, D., *Top. Catal*., 2004, vol. 30/31, p. 27.
18. Hernández Carucci, J.R., Arve, K., Eränen, K., Murzin, D.Yu., and Salmi, T., *Catal. Today*, 2008, vols. 133−135, p. 448.
19. Meunier, F.C., Breen, J.P., Zuzaniuk, V., Olsson, M., and Ross, J.R.H., *J. Catal*., 1999, vol. 187, p. 493.
20. Eränen, K., Klingstedt, F., Arve, K., Lindfors, L.E., and Murzin, D.Yu., *J. Catal*., 2004, vol. 227, p. 328.
21. *http://www.sriconsulting.com/WP/Public/Reports/eo/.*
22. Rebsdat, S. and Mayer, D., *Ethylene Oxide,* in *Ullman's Encyclopedia of Industrial Technology*, 7th ed., Weinheim: Wiley−VCH, 2005 (Online electronic ed.).
23. Gavriilidis, A., Angeli, P., Cao, E., Yeong, K.K., and Wan, Y.S.S., *Chem. Eng. Res. Des*., 2002, vol. 80, p. 3.
24. Stankiewicz, I. And Moulijn, J.A., *Chem. Eng. Prog*., 2000, vol. 96, p. 22.
25. Nault, L.G., Bolme, D.W., and Johanson, L.N., *Ind. Eng. Chem. Process Des. Dev*., 1962, vol. 1, p. 285.
26. van Santen, R.A. and Kuipers, H.P.C.E., *Adv. Catal.*, 1987, vol. 35, p. 265.
27. Campbell, T., *J. Catal*., 1985, vol. 94, p. 436.
28. Kestenbaum, H., Lange de Oliveira, A., Schmidt, W., Schuth, F., Ehrfeld, W., Gebauer, K., Löwe, H., and Richter, T., *Stud. Surf. Sci. Catal*., 2000, vol. 130, p. 2741.
29. Lee, J.K., Verykios, X.E., and Pitchai, R., *Appl. Catal*., 1988, vol. 44, p. 223.
30. Levenspiel, O., *The Chemical Reactor Omnibook*, Corvallis: Oregon State Univ. Bookstores, 1989.
31. Obuchi, A., Ohi, A., Nakamura, M., Ogata, A., Mizuno, K., and Ohuchi, H., *Appl. Catal. B: Environ.*, 1993, vol. 2, p. 71.
32. Danckwerts, P.V., *Chem. Eng. Sci*., 1953, vol. 2, p. 1.
33. Garcia, J., Garcia, E., Hyde, J.R., Fraga, J., Yan, C., Poliakoff, M., and Cocero, M.J., *J. Supercrit. Fluids*, 2007, vol. 41, p. 82.
34. Westerterp, R., van Swaaij, W.P.M., and Beenackers, A.C.M., *Chemical Reactor Design and Operation*, Amsterdam: Elsevier, 1984.
35. Sotowa, K., Kusakabe, K., and Street, D., *Fluent News*, 2002, vol. 11, p. 18.
36. Hardt, S., *Modeling and Simulation of Microreactors in Modeling of Process Intensification*, Keil, F.J., Ed., Weinheim: Wiley-VCH, 2007.
37. Roy, S. and Raju, R., *J. Appl. Phys.*, 2003, vol. 93, p. 4870.
38. Hernández Carucci, J.R., Eränen, K., Murzin, D.Yu., and Salmi, T.O., *Catal. Today*, 2009, vol. 147, p. S149.
39. Hayes, R.E., Liu, B., Moxom, R., and Votsmeier, M., *Chem. Eng. Sci*., 2004, vol. 59, p. 3169.
40. Gobby, D. Eames, I, and Gavriilidis, A., *Proc. 5th Int. Conf. on Microreaction Technology (IMRET 5)*, Berlin: Springer, 2001, p. 141
41. Schouten, P.S., Borman, P.C., and Westerterp, K.R., *Chem. Eng. Process*, 1996, vol. 35, p. 43.
42. Haario, H., *ModEst 6.0 – A User's Guide,* Helsinki: ProfMath, 2007.
43. Arve, K., Backman, H., Klingstedt, F., Eränen, K., and Murzin, D.Yu., *Appl. Catal*. A: *Gen.,* 2006, vol. 303, p. 96.
44. Marnellos, G.E., Efthimiadis, E.A., and Vasalos, I.A., *Appl. Catal. B: Environ.*, 2004, vol. 48, p. 1.

45. Murzin, Yu., Kubickova, I., Snåre, M., and Mäki-Arvela, P., EU Patent 05075068.6, 2005.
46. Arve, K., Hernández Carucci, J.R., Eränen, K., Aho, A., and Murzin, D.Yu., *Appl. Catal. B: Environmental*, 2009, vol. 90, p. 603.
47. Hernández Carucci, J.R., Kurman, A., Karhu, H., Arve, K., Eränen, K., Wärnå, J., Salmi, T., and Murzin, D.Yu., *Chem. Eng. J*., 2009, vol. 154, p. 34.
48. Temkin, M.I., *Adv. Catal.*, 1979, vol. 28, p. 173.
49. Laidler, K.J., *Chemical Kinetics,* New York: Harper and Row, 1987, 3rd ed.
50. Stegelmann, C., Schiodt, N.C., Campbell, C.T., and Stoltze, P., *J. Catal*., 2004, vol. 221, p. 630.
51. Petrov, L., Eliyas, A., and Shopov, D., *Appl. Catal*., 1985, vol. 18, p. 87.
52. Lafarga, D., Al-Juaied, M.A., Bondy, C.M., and Varma, A., *Ind. Eng. Chem. Res*., 2000, vol. 39, p. 2148.
53. Borman, P.C. and Westerterp, K.R., *Ind. Eng. Chem. Res*., 1995, vol. 34, p. 49.
54. Schouten, P.S., Borman, P.C., and Westerterp, K.R., *Chem. Eng. Process*., 1996, vol. 35, p. 107.
55. Kestenbaum, H., Lange de Oliveira, A., Schmidt, W., Schüth, F., Ehrfeld, W., Gebauer, K., Löwe, H., Richter, T., Lebiedz, D., Untiedt, I., and Züchner, H., *Ind. Eng. Chem. Res*., 2002, vol. 41, p. 710.
56. Kim, Y.-C., Park, N.-C., Shin, J.-S., Lee, S.R., Lee, Y.J., and Moon, D.J., *Catal. Today*, 2003, vol. 87, p. 153.
57. Gleaves, J.T., Sault, A.G., Madix, R.J., and Ebner, J.R., *J. Catal*., 1990, vol. 121, p. 202.
58. Stegelmann, C. And Stoltze, P., *Ibid.*, 2004, vol. 226, p. 129.
59. Vayenas, C.G., Bebelis, S., Pliangos, C., Brosda, S., and Tsiplakides, D., *Electrochemical Activation of Catalysis: Promotion, Electrochemical Promotion, and Metal-Support Interactions*, New York: Kluwer, 2002.